nanomaterials

MDPI

Review

Emerging and Promising Multifunctional Nanomaterial for Textile Application Based on Graphitic Carbon Nitride Heterostructure Nanocomposites

Dominika Glažar [1], Ivan Jerman [2], Brigita Tomšič [1], Raghuraj Singh Chouhan [3] and Barbara Simončič [1,*]

[1] Faculty of Natural Sciences and Engineering, University of Ljubljana, Aškerčeva Cesta 12, 1000 Ljubljana, Slovenia
[2] National Institute of Chemistry, Hajdrihova 19, 1000 Ljubljana, Slovenia
[3] Jožef Stefan Institute, Department of Environmental Sciences, Jamova Cesta 3, 1000 Ljubljana, Slovenia
* Correspondence: barbara.simoncic@ntf.uni-lj.si

Abstract: Nanocomposites constructed with heterostructures of graphitic carbon nitride (g-C_3N_4), silver (Ag), and titanium dioxide (TiO_2) have emerged as promising nanomaterials for various environmental, energy, and clinical applications. In the field of textiles, Ag and TiO_2 are already recognized as essential nanomaterials for the chemical surface and bulk modification of various textile materials, but the application of composites with g-C_3N_4 as a green and visible-light-active photocatalyst has not yet been fully established. This review provides an overview of the construction of Ag/g-C_3N_4, TiO_2/g-C_3N_4, and Ag/TiO_2/g-C_3N_4 heterostructures; the mechanisms of their photocatalytic activity; and the application of photocatalytic textile platforms in the photochemical activation of organic synthesis, energy generation, and the removal of various organic pollutants from water. Future prospects for the functionalization of textiles using g-C_3N_4-containing heterostructures with Ag and TiO_2 are highlighted.

Keywords: g-C_3N_4; Ag; TiO_2; nanomaterial; heterostructures; textile; functionalization

Citation: Glažar, D.; Jerman, I.; Tomšič, B.; Chouhan, R.S.; Simončič, B. Emerging and Promising Multifunctional Nanomaterial for Textile Application Based on Graphitic Carbon Nitride Heterostructure Nanocomposites. *Nanomaterials* **2023**, *13*, 408. https://doi.org/10.3390/nano13030408

Academic Editors: Vincenzo Vaiano and Antonio Di Bartolomeo

Received: 30 December 2022
Revised: 14 January 2023
Accepted: 17 January 2023
Published: 19 January 2023

1. Introduction

As a next-generation visible-light-active photocatalyst, graphitic carbon nitride (g-C_3N_4) has attracted considerable attention in various scientific fields, including environment remediation [1–11], energy storage and conversion [4,5,8,12–17], and biomedicine [18–20], which are the most important applications. It has already emerged as a promising nanomaterial for the degradation of various organic and inorganic environmental pollutants [1–6,8–11], CO_2 reduction [3,8,15], NO_x removal [3], hydrogen evolution through water splitting [3,4,8,12–16], supercapacitors and batteries [5,8], solar and fuel cells [17], diagnostic imaging [19], therapeutic applications [19,20], biosensors [4,7,18–20], and antibacterial disinfection [3,19,20]. Accordingly, there have been a large number of scientific publications on g-C_3N_4 and g-C_3N_4 heterostructures, including more than 2000 original and review articles in 2022 alone (source: Web of Science, advanced search query preview: "graphitic carbon nitride or g-C_3N_4" and "photocataly*" in abstracts in 2022, assessed on 28 December 2022).

The attractiveness of g-C_3N_4 is directly related to its properties, as it is distinguished as a sustainable, organic, and metal-free two-dimensional conjugated polymeric n-type semiconductor with unique optical and electronic properties, high physicochemical and thermal stability, and high corrosion resistance, in addition to having a high earth abundance and an easy and inexpensive means of fabrication [21]. Due to its mild band gap of about 2.7 eV, g-C_3N_4 responds to visible light with an optical absorption edge of about 460 nm and, therefore, enables visible-light-driven photocatalytic reactions [22,23]. Pure g-C_3N_4 consists of carbon and nitrogen elements and is usually prepared through thermal polycondensation from nitrogen-rich precursors, such as melamine, urea, thiourea,

dicyandiamide, cyanamide, and cyanuric acid, in the temperature range between 450 °C and 650 °C (Figure 1a,b) [8,22,24–27]. It has a graphite-like layered structure composed of aromatic s-triazine (C_3N_4) (Figure 1c) and tri-s-triazine (C_6N_7) (Figure 1d) rings linked by tertiary amines. The layers are held together by weak van der Waals forces. Since g-C_3N_4 synthesized in this way is bulky and exhibits low surface area, marginal optical absorption in the visible region, rapid charge recombination, and low charge mobility, various nanostructured forms of g-C_3N_4 in different morphologies with higher photocatalytic activity have been prepared, including 3D porous structures, 2D nanosheets, 1D nanorods/nanotubes, and 0D g-C_3N_4 quantum nanodots [4,7,21,25].

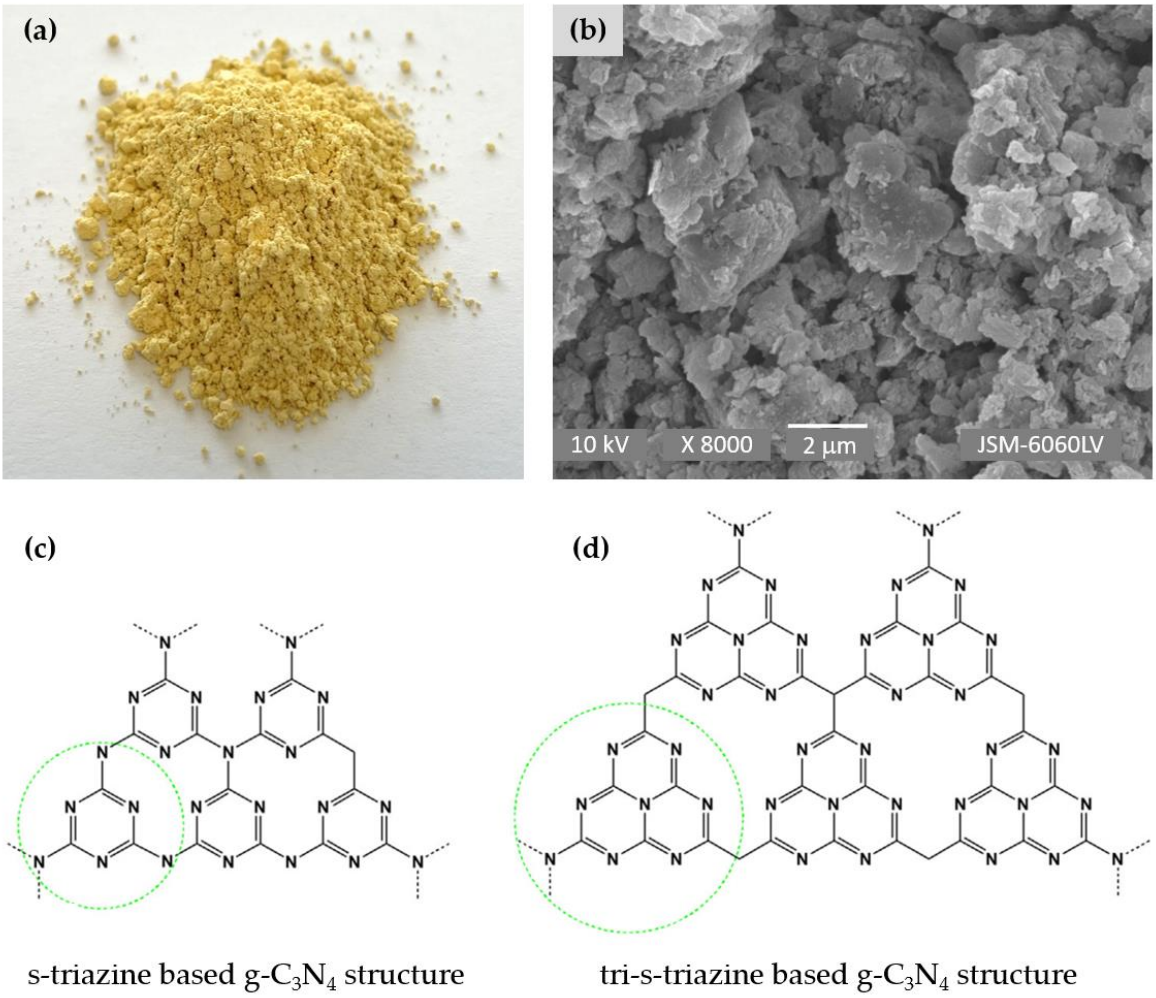

Figure 1. Schematic presentation of g-C_3N_4: photo of g-C_3N_4 powder (**a**), SEM image of g-C_3N_4 nanosheets (**b**), s-triazine (**c**), and tri-s-triazine (**d**) structure of g-C_3N_4. Reprinted with permission from [19]. Copyright 2020, Elsevier.

Another important strategy to improve the photocatalytic efficiency of g-C_3N_4 is the formation of g-C_3N_4-based binary and ternary heterostructure composites, including doping/loading with noble metals and creating heterojunctions with other organic and inorganic semiconductors [15,28]. Recently, for example, various heterostructure composites, such as Ag/g-C_3N_4 [29–31], Au/g-C_3N_4 [31–33], graphene oxide/g-C_3N_4 [34–37], TiO_2/g-C_3N_4 [38–42], Ag/TiO_2/g-C_3N_4 [43–45], TiO_2/Cu/g-C_3N_4 [46], TiO_2/ZrO_2/g-C_3N_4 [47], and Bi_2WO_6/g-C_3N_4/TiO_2 [48] have been successfully prepared, to optimize the optical properties of g-C_3N_4 and significantly improve its overall photocatalytic activity.

g-C_3N_4 and g-C_3N_4-containing heterostructure composites have also become important materials in the field of textiles and can be beneficially used for the degradation of

pollutants in textile wastewater or for the chemical modification of textile fibers, to create different functionalities [11]. Natural and synthetic textile fibers are an ideal material for the fabrication of textile-based photocatalytic platforms, because they have advantages over other solid substrates, such as flexibility, lightness, porosity, absorptivity, and wearability. However, while the photocatalytic degradation of different dyes through the presence of g-C_3N_4 alone or its heterostructure composites has become a widely used sustainable strategy for the purification of dye wastewater [11], the functionalization of textile fibers with g-C_3N_4-containing materials remains challenging and, therefore, a topic of research [27]. There are 65 publications dealing with the use of g-C_3N_4 and g-C_3N_4 heterostructures for textile applications (Source: Web of Science, advanced search query preview: "graphitic carbon nitride or g-C_3N_4" and "textile or fabric" in abstracts, assessed on 28 December 2022), but most of these studies deal with the removal of textile dyes from wastewater. Therefore, it is of great importance to investigate the advantages of g-C_3N_4 and g-C_3N_4-containing heterostructure composites as promising "green" materials for textile functionalization.

In our previous review paper [27], we presented g-C_3N_4 as a new sustainable photocatalyst for textile functionalization, focusing on the textile substrates used, the application methods, and the developed functionalities, such as photocatalytic self-cleaning, antibacterial, and flame-retardant properties, as well as the creation of a textile catalytic platform for water disinfection, removal of various organic pollutants from water, and selective organic matter transformations. To provide additional valuable information on the recent advances in surface and bulk modification of textile fibers by g-C_3N_4-containing nanomaterials, this review article focuses on the application of heterostructure nanocomposites of g-C_3N_4 with Ag and TiO_2 nanoparticles (NPs), as the most popular and widely used nanomaterials for surface and bulk chemical modification of textiles [49]. In the literature, both binary and ternary heterostructure composites, including Ag/g-C_3N_4, TiO_2/g-C_3N_4, and Ag/TiO_2/g-C_3N_4 have been considered promising functional nanomaterials, because the synergistic effect of the components in the heterostructures leads to the enhanced photocatalytic performance of the composites compared with the single-component materials. In this review, the processes for the synthesis of Ag/g-C_3N_4, TiO_2/g-C_3N_4, and Ag/TiO_2/g-C_3N_4 nanocomposites are explained, while their potential photocatalytic mechanisms of action and the developed functionalities on textile fibers for photochemical activation of organic synthesis, energy generation, and the removal of various organic pollutants, as well as future prospects, are highlighted.

2. Ag/g-C_3N_4 Nanocomposites

2.1. Preparation and Photocatalytic Mechanism of Ag/g-C_3N_4 Nanocomposites

As a superior multifunctional nanomaterial, Ag NPs are attractive candidates for surface loading or doping to develop noble metal/semiconductor heterostructures, also referred to as Ag/g-C_3N_4 [50,51]. The Ag/g-C_3N_4 nanocomposites exhibit not only enhanced visible light photocatalytic performance, but also improved antimicrobial performance due to the excellent antimicrobial activity of Ag against a wide range of Gram-negative and Gram-positive bacteria, viruses, fungi, molds, yeasts, and algae [52]. Ag/g-C_3N_4 nanocomposites have already been used for the degradation of environmental pollutants, such as in the decolourization of different dyes [30,53–58] and the degradation of organic solvents [53,59–61] and antibiotics [62–65]. They have also been used in hydrogen generation [66]; in microbial disinfection [57,67,68]; and as chemical sensors to detect drugs [69,70], biothiols [71], plant pigments [72], and pesticides [61]. In another case, Ag/g-C_3N_4 was used to obtain composites with multiple colors [73].

Two different approaches have been used to prepare Ag/g-C_3N_4 nanocomposites, namely one-step and two-step processes, the latter of which is more commonly used. In the two-step process [30,53–57,59,61,63,65,67,69–73], g-C_3N_4 is first synthesized from a suitable precursor in the form of bulk material, g-C_3N_4 nanosheets, or g-C_3N_4 quantum dots. Then, g-C_3N_4 is dispersed in the water medium and mixed with $AgNO_3$, which serves as a precursor for Ag NPs. Subsequently, Ag NPs are synthesized in the pres-

ence of g-C_3N_4 using various reducing agents, such as $NaBH_4$ [30,59,61,65], hydrazine hydrate [70], sodium citrate [72], plant extracts [54], and UV light [53,55,63,67,73]. In this case, g-C_3N_4 serves as a platform for the synthesis of Ag NPs, and its surface is decorated with Ag^0 (Figure 2a). On the other hand, in the one-step process [56,57,62,74], urea or a mixture of melamine and cyanuric acid are used as g-C_3N_4 precursors and mixed with $AgNO_3$ in a suitable medium, and the simultaneous synthesis of Ag NPs/g-C_3N_4 is carried out under appropriate conditions. This synthesis procedure enables the preparation of Ag-doped g-C_3N_4.

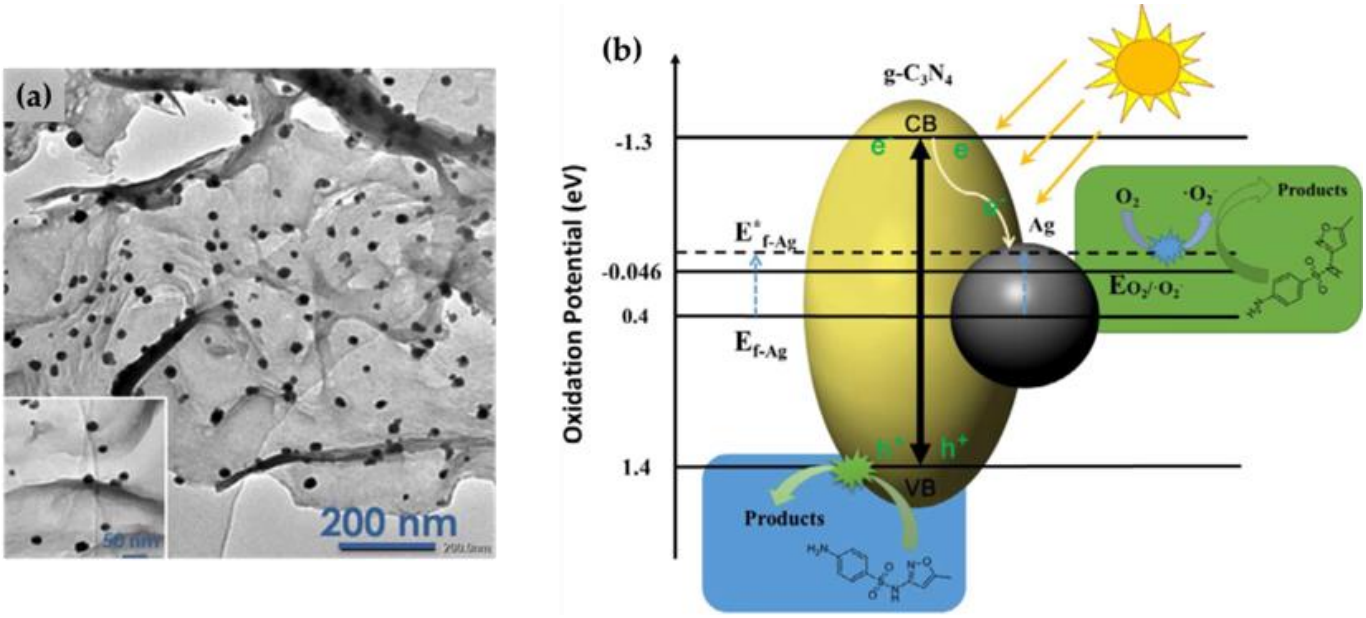

Figure 2. TEM image of Ag/g-C_3N_4 nanocomposite (**a**), photocatalytic mechanism of the Ag/g-C_3N_4 heterostructure (**b**). Reprinted with permission from [63]. Copyright 2018, Elsevier.

The proposed mechanism behind the photocatalytic activity of the Ag/g-C_3N_4 nanocomposite is shown in Figure 2b [53,54,56,57,59,63,75,76]. It is believed that the photocatalytic efficiency of the noble metal/semiconductor heterostructure composite is significantly enhanced by the presence of Ag^0, which acts as a current collector and plasmonic absorber [77].

Ag/g-C_3N_4 nanocomposite is a visible-light photocatalyst. According to the literature [23], the band gap energy of g-C_3N_4 is 2.7 eV, with the potentials of the valence band (VB) and conduction band (CB) being 1.4 eV and −1.3 eV, respectively. Irradiation with energy higher than the band gap energy of g-C_3N_4 results in the excitation of electrons (e^-) from VB to CB, leaving holes (h^+) in VB. The photogenerated e^- in CB of g-C_3N_4 can be easily transferred to the Ag NPs because the Fermi level of Ag is less negative compared with the CB of g-C_3N_4. This creates a Schottky barrier that maximizes photoinduced charge carrier separation and prevents recombination of the e^--h^+ pair. The injected e^- accumulates on Ag and can easily enter the reduction reactions on the surface, such as the reduction of O_2 to superoxide radicals ($\bullet O_2^-$) [63] or the reduction of H^+ to H_2 in hydrogen production by water splitting [76]. At the same time, visible light leads to the excitation of e^- in the Ag surface layer, resulting in surface plasmon resonance (SPR). The generation of SPR can greatly enhance the photoactivity of the composite through the mechanism of plasmon resonance energy transfer [77], because the intense near-electric field induced by SPR improves the efficiency of charge carrier separation [33] and increases the rate of charge carrier formation in g-C_3N_4 [44]. On the other hand, h^+ in VB can directly oxidize different pollutants [57,63], but h^+ cannot oxidize ^-OH to give $\bullet OH$ radicals, since the VB edge potential of g-C_3N_4 is less positive than the standard redox potential of $^-OH/\bullet OH$

(+1.99 eV) [53,57,63,75]. This means that •OH radicals cannot be directly generated in the photochemical process of g-C_3N_4.

2.2. Ag/g-C_3N_4 Nanocomposites for Textile Application

Chemically modified textile substrates with Ag/g-C_3N_4 nanocomposites have been advantageously used in the photocatalysis of various organic reactions [78,79] and textile-based triboelectric nanogenerators [80]. While the first application involves photochemical activation of organic synthesis without additional reagents, thus providing a more environmentally friendly route for organic chemical conversion, the second application represents an emerging textile-based energy-harvesting device, as a potential power source for wearable electronics.

New functionality was imparted to a polyester (PES) fabric by dip-coating with g-C_3N_4 nanosheets under ultrasonic treatment, followed by in situ synthesis of Ag NPs in an aqueous solution of $AgNO_3$ of different concentrations (3–10 wt%), using $NaBH_4$ as a reducing agent [79]. From the SEM images, it is evident that the micro smooth morphology of the PES fibers (Figure 3a) was completely changed by the application of the g-C_3N_4 nanosheets (Figure 3b), as well as the Ag/g-C_3N_4 nanocomposite (Figure 3c). The latter became microrough, with clearly visible deposited and uniformly distributed spherical Ag^0 particles with an average size of 13.3 nm. The crystalline phase of the uncoated and coated PES samples was determined by X-ray diffraction (Figure 3d). Since the characteristic diffraction peaks of g-C_3N_4 at 2θ~27.5° and 13.1° could not be detected in the XRD pattern of the PES sample, the presence of Ag^0 showed four peaks at 2θ = 37.47°, 43.69°, 63.97°, and 77.02°, corresponding to the cubic Ag^0 planes (111), (200), (220), and (311), respectively. It is also evident that the application of g-C_3N_4 nanosheets changed the white color of the PES fabric to brown, but the in situ synthesis of Ag NPs to grey (Figure 3e).

PES coated with g-C_3N_4 and Ag/g-C_3N_4 nanocomposites, containing different amounts of Ag^0 from 3 to 10 wt%, was used as a sustainable chemical catalyst for the hydrogenation of 4-nitrophenol, one of the most toxic organic pollutants in industrial wastewater, into the valuable compound 4-aminophenol, using $NaBH_4$ as the hydride source [79]. Since a one-component g-C_3N_4 coating on PES fabric does not act as a catalyst for the conversion of 4-nitrophenol into 4-aminophenol, the presence of 3 wt% Ag^0 in the Ag/g-C_3N_4 nanocomposite resulted in a 30% conversion of 4-nitrophenol into 4-aminophenol after a reaction time of 5 min, and this increased to 90% conversion when the Ag loading was increased to 10 wt%, with an apparent rate constant of 0.462 min^{-1}, which is more than six-times higher than that of 3 wt% Ag^0. (Figure 3f). This indicates that Ag NPs facilitated the electron transfer from BH_4^- to 4-nitrophenolate, thus lowering the barrier of activation energy for the reduction of 4-nitrophenol to 4-aminophenol (Figure 3g). The high recyclability and stability of the catalyst was evidenced by the fact that the catalytic performance of the catalyst was still nearly 90% after 10 cycles. A comparison with some other Ag-based catalysts from the literature clearly showed that the conversion of 4-nitrophenol over Ag/g-C_3N_4 coated PES exhibited enhanced the catalytic activity and recyclability [79].

Ag NP-decorated g-C_3N_4 was also used in the bulk modification of polyacrylonitrile nanofibers (PAN NFs) for selective oxidation of styrene, benzylic methylene groups, and benzene into the desired products under visible light irradiation and milder reaction conditions [78]. For this purpose, Ag NPs/g-C_3N_4 composite and 10 wt% PAN were dispersed in an organic solvent under sonification, to produce a homogeneous polymer solution, which was then electrospun to produce PAN NFs with the embedded Ag NPs/g-C_3N_4 (Figure 4a,b). TEM micrography showed small dark particles and bulges on the PAN NFs, indicating that the Ag NPs/g-C_3N_4 was well dispersed on the PAN surface or embedded in the PAN matrix, without agglomerating (Figure 4b). The as-prepared PAN/Ag NPs/g-C_3N_4 NFs exhibited a highly porous nature with excellent absorption performance. To optimize the photooxidation reactions, the influence of different parameters, such as the amount of PAN/Ag NPs/g-C_3N_4 NFs, organic solvents, reaction time, the presence or absence of visible light (domestic bulb (40 w)), and H_2O_2 as oxidant, on the photocatalytic

performance was investigated. It was found that the oxidation selectivity and conversion increased with the increase in catalyst concentration and reaction time in the organic solvent acetonitrile, as well as in the presence of light and H_2O_2. In this case, a 98% conversion of styrene and 60% selectivity toward styrene oxide (Figure 4c), 98% conversion of ethylbenzene and 99% selectivity toward acetophenone (Figure 4d), as well as an excellent 99% conversion of benzene into the desired phenol, was obtained using H_2O_2 as oxidant (Figure 4e) under optimized reaction conditions (Figure 4f). A recyclability study of the PAN/Ag NPs/g-C_3N_4 NFs for styrene oxidation showed that the catalyst exhibited high reusability activity with a product yield of more than 85% in a repeat test of five runs.

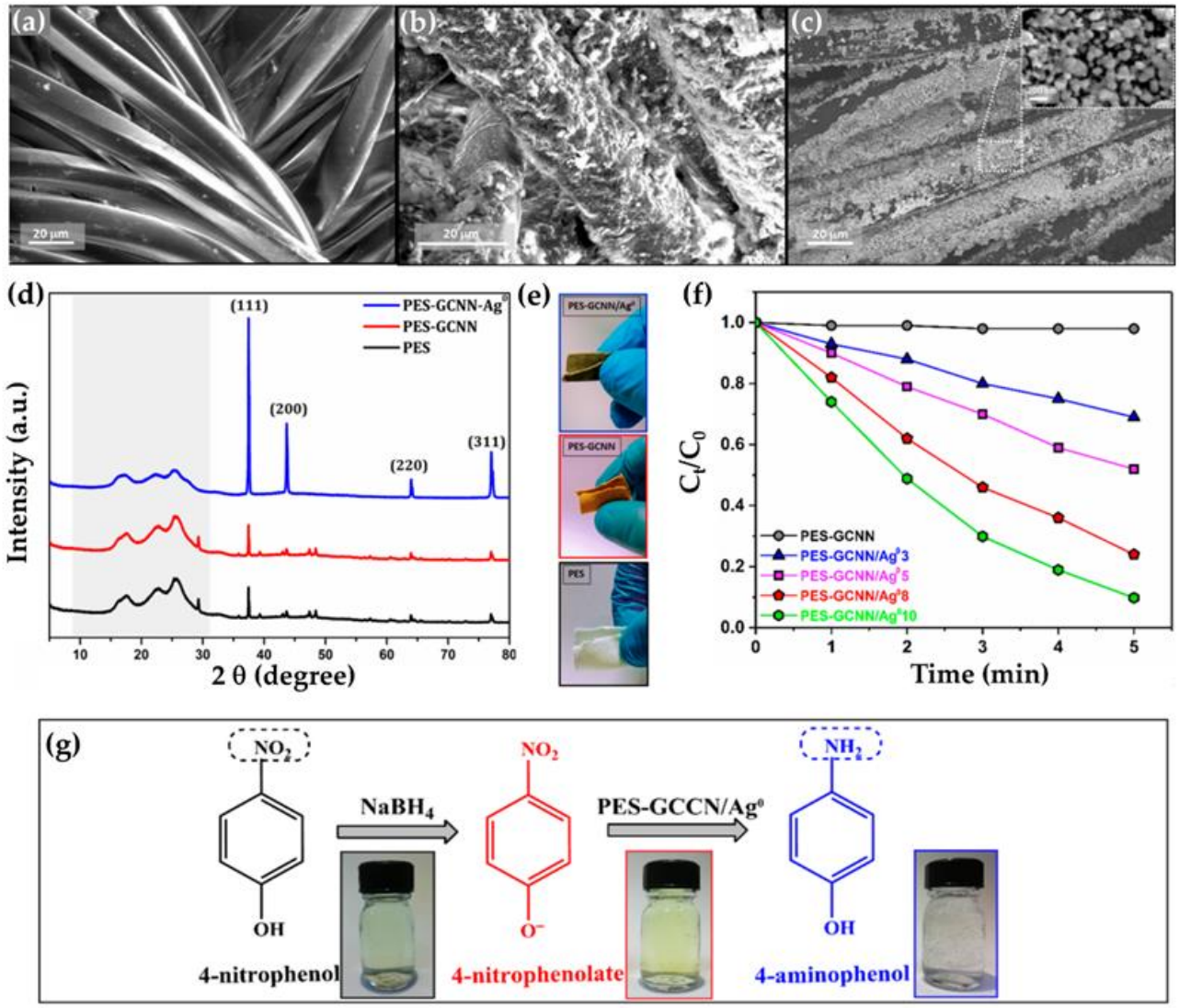

Figure 3. SEM images of uncoated PES fabric (**a**), PES coated with g-C_3N_4 (PES-GCNN sample) (**b**), and PES coated with Ag/g-C_3N_4 nanocomposite containing 10 wt% of Ag^0 (PES-GCNN-Ag^0 10) (**c**); XRD patterns of PES, PES-GCNN, and PES-GCNN-Ag^0 10 samples (**d**); photos of PES, PES-GCNN, and PES-GCNN-Ag^0 10 samples (**e**); time-dependent 4-NP conversion over PES-GCNN-Ag^0 samples containing 3, 5, 8, and 10 wt% of Ag^0 (**f**); reaction scheme and photographs representing reduction of 4-NP to 4-AP by $NaBH_4$ catalyzed by PES-GCNN-Ag^0 (**g**). Reprinted with permission from [79]. Copyright 2021, MDPI.

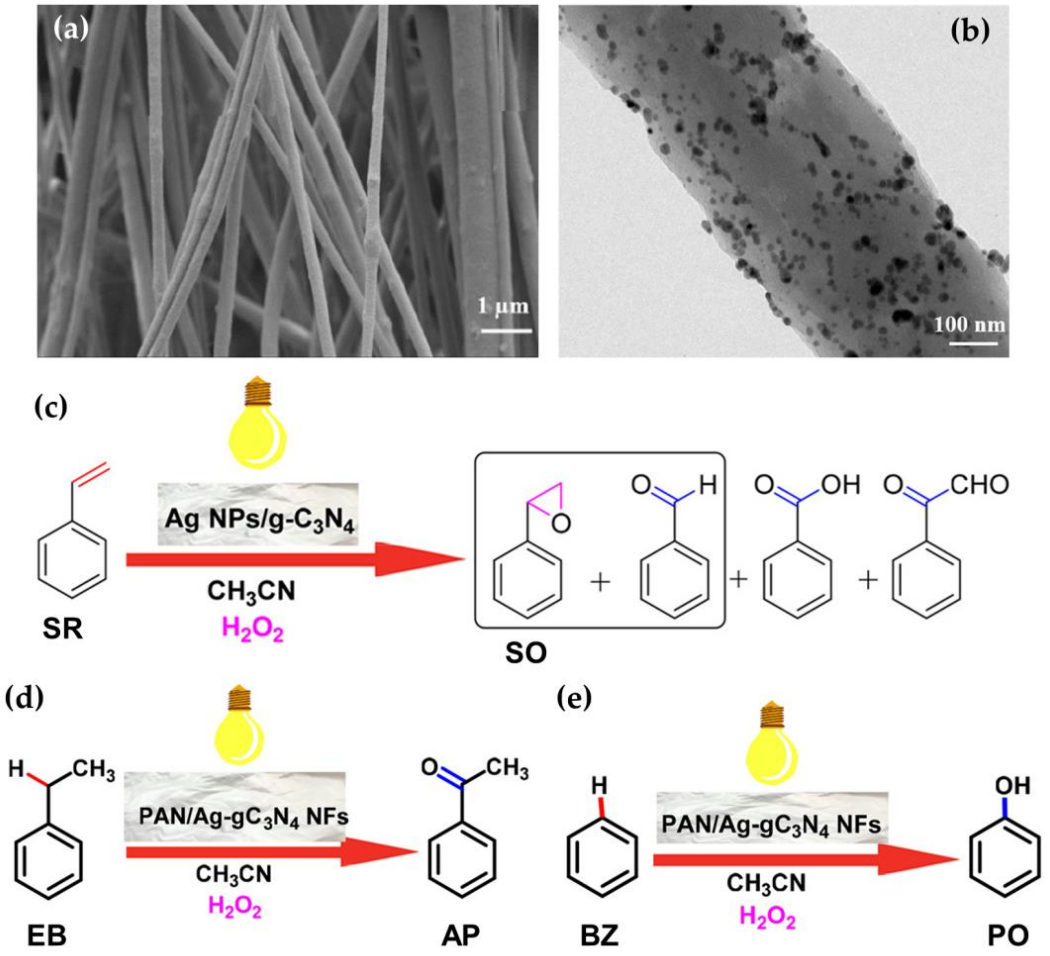

(f) Optimised reaction conditions					
Oxidation reaction	Catalyst mass (mg)	Reaction time (h)	Conversion (%)	Selectivity (%)	TOF (h^{-1})
SR to SO	20	16	98	60	9.23
EB to AP	20	12	98	99	16.5
BZ to PO	20	0.5	99	/*	398

* No data

Figure 4. SEM (**a**) and TEM (**b**) images of PAN NFs with the embedded Ag NPs/g-C_3N_4; schematic presentation of oxidation of styrene (SR) to styrene oxide (SO) (**c**), selective oxidation of ethylbenzene (EB) to acetophenone (AP) (**d**), and selective oxidation of benzene (BZ) to phenol (PN) (**e**) by PAN NFs, with the embedded Ag NPs/g-C_3N_4 as a catalyst under visible light irradiation, and optimized reaction conditions with the turnover frequency (TOF) values (**f**). Reprinted with permission from [78]. Copyright 2020, ACS.

Recently, a textile-based triboelectric nanogenerator (T-TENG) for mechanical energy harvesting was fabricated by depositing an active layer of g-C_3N_4 nanosheets decorated with Ag NPs on a nylon-coated conductive carbon fabric as a textile backbone (Figure 5a–c), using Teflon or polypropylene as a counter triboelectric material [80]. To establish electrical contact, aluminum adhesive tapes were attached on one of the surfaces of these layers, with an extension for electrical contacts. To produce a voltage, the fabric based samples and Teflon were put in repetitive contact-separation mode through mechanical agitation. When the two materials are in contact, charge transfer occurs between the two surfaces, and when the two materials are separated, a current flows through the external circuit, to

balance the potential on the two surfaces. Such a configuration of an Ag/g-C_3N_4/nylon bi-layer T-TENG generates an open circuit voltage of ~200 V, which is more than 10 times higher compared with a bare g-C_3N_4 nanosheet layer (19 V) and almost four-times higher compared to a g-C_3N_4/nylon bi-layer (52 V) (Figure 5d). The thermal stability, as well as the conversion efficiency, at an elevated temperature of up to ~65 °C make it a potential candidate for integration into textile-based wearable electronic devices (Figure 5e). The synergistic effect of interfacial charge trapping, the increased surface area and the increased surface charge density in the Ag/g-C_3N_4/nylon bi-layer system result in the development of a maximum short circuit current of ~1.1 μA, which is about three-times higher than that of g-C_3N_4/nylon (Figure 5f) and delivery of a maximum output power of ~3.1 μW/cm^2, which is higher than that obtained from g-C_3N_4/nylon (Figure 5g). When a Ag/g-C_3N_4/nylon bi-layer T-TENG was examined upon charging a commercial capacitor (0.26 μF) using a bridge rectifier, the Ag/g-C_3N_4/nylon device was able to charge the capacitor to ~85 V within 30 s, which is more than 2.7 times higher than the result of a g-C_3N_4/nylon device (Figure 5h). In addition, several commercially available LEDs could be driven by the capacitors, which were charged by the impact of the textile-based nanogenerator (insert in Figure 5h). The excellent power generation capability of this fabric coated with an Ag/g-C_3N_4/nylon bi-layer indicates its potential applicability for wearable and flexible nanogenerators.

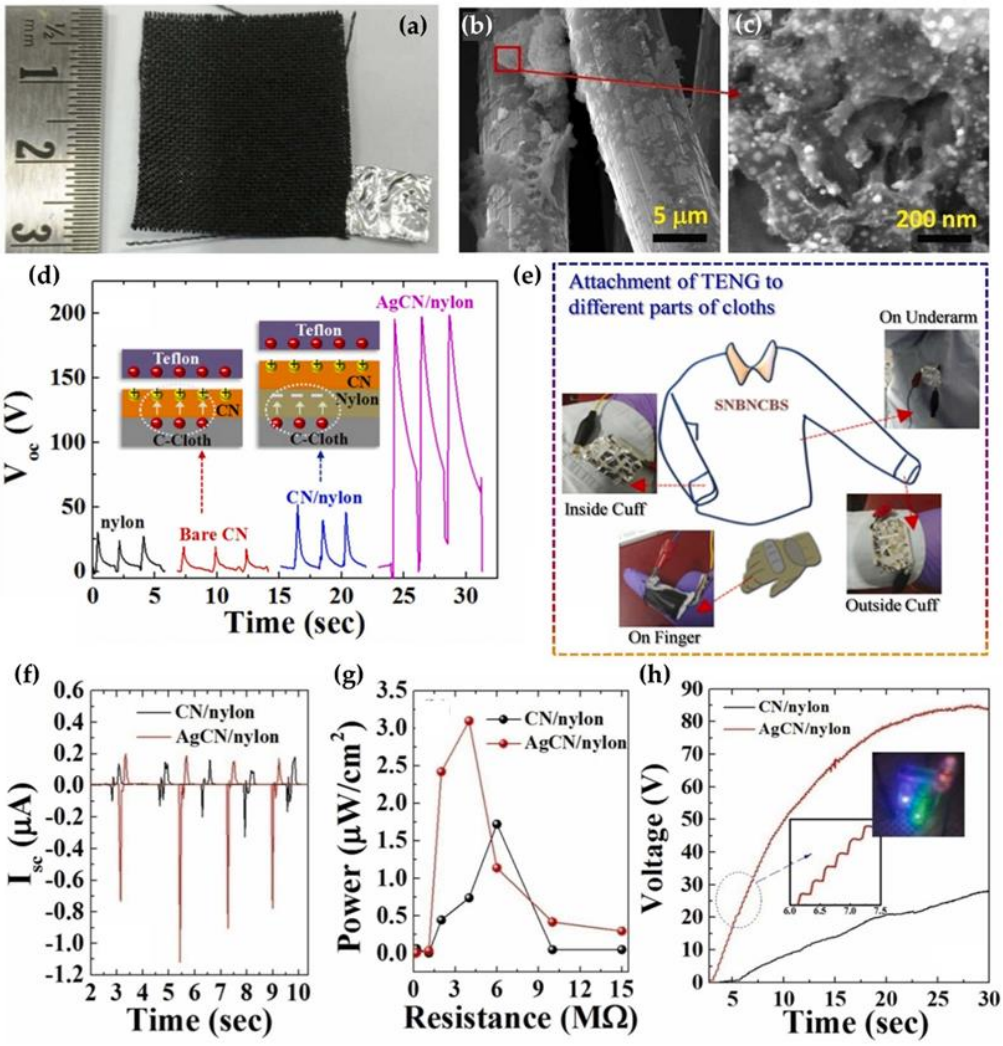

Figure 5. Photograph of an Ag/g-C_3N_4/nylon coated C-cloth with Al electrode (**a**); SEM images of Ag/g-C_3N_4 decorated on nylon coated C-cloth under lower and higher magnification (**b**,**c**); open circuit

voltage generation from TENG operation for different layers with Teflon as a counter triboelectric material under a mechanical impact (**d**); attachment of TENG to different parts of clothes (**e**); short circuit current (**f**), output power density (**g**), and capacitor charging voltage (**h**) for g-C_3N_4/nylon and Ag/g-C_3N_4/nylon based T-TENGs (insets show a closer view of voltage profile and the glowing of LEDs using the charged capacitor). Reprinted with permission from [80]. Copyright 2022, Elsevier.

3. TiO_2/g-C_3N_4 Heterojunctions

3.1. Preparation and Photocatalytic Mechanism of TiO_2/g-C_3N_4 Nanocomposites

The design and construction of TiO_2/g-C_3N_4 hybrid photocatalysts have attracted much attention, as they have been recognized as an effective material for various environmental and energy applications [81–98]. It should be noted that TiO_2 in the TiO_2/g-C_3N_4 heterojunction is a wide-band-gap semiconductor that responds to UV light (Eg = 3.2 eV; $\lambda \leq 387.5$ nm) [99,100], while g-C_3N_4 responds to visible light. It is believed that the formation of a synergistic TiO_2/g-C_3N_4 heterojunction can significantly reduce the recombination of photogenerated electron–hole pairs and increase the photocatalytic activity of TiO_2 in visible light, which is beneficial for both photocatalysts [92,101]. Moreover, the TiO_2/g-C_3N_4 heterojunction is expected to simultaneously utilize UV and visible light, thus exhibiting excellent photocatalytic performance under UV and visible light irradiation [82,92].

In the preparation of a TiO_2/g-C_3N_4 heterojunction, two-step processes have generally been applied in two different ways [82–88,91–98]. The first approach involves the prior synthesis of both TiO_2 and g-C_3N_4 from the corresponding precursors and subsequent mixing [87,88,92,95–98]. In the other approach, in situ synthesis of TiO_2 was performed in the presence of presynthesized g-C_3N_4 [82–86,93,94] or conversely, the in situ synthesis of g-C_3N_4 was performed in the presence of presynthesized TiO_2 [91]. While urea [84,85,88,91,92,95], melamine [82,86,93,94,96,97], dicyandiamide [87,98], or a combination of urea and melamine [83] have been used as precursors for g-C_3N_4 synthesis, titanium(IV) butoxide [85,92,93,95,96], titanium(IV) isopropoxide [84], titanium tetrachloride [82,83,86], titanium(IV) bis-(ammonium lactato) dihydroxide [94], and titanyl sulphate [97] are widely used as TiO_2 precursors. For TiO_2 synthesis, the hydrothermal or solvothermal assisted sol-gel process under acidic or alkaline conditions is mostly used [82,84,86,87,92,93,96]. In addition to the two-step processes, a one-step hydrothermal process using melamine as g-C_3N_4 precursor and titanium(IV) isopropoxide as TiO_2 precursor and cyanuric acid as catalyst has also been reported [90]. All the above processes are completed by drying and calcining the nanocomposites under suitable conditions, to obtain the desired morphology.

Two mechanisms have been proposed for the photocatalytic activity of TiO_2/g-C_3N_4 nanocomposites, including the Type-II heterojunction (Figure 6a) [82,87,92–94,96–98,102] and the direct Z-scheme (Figure 6b) [90,91,95]. In both mechanisms, it is assumed that when g-C_3N_4 and TiO_2 are excited in the heterojunction by incident UV/visible light of sufficient energy, the photoinduced electrons are transferred from VB to CB, leaving holes in VB. According to the Type-II heterojunction mechanism, the photogenerated electrons can be easily transferred from CB of g-C_3N_4 to CB of TiO_2 because the CB edge potential of g-C_3N_4 (−1.3 eV) is more negative than that of TiO_2 (−0.29 eV). At the same time, the photogenerated holes can be transferred from VB of TiO_2 to VB of g-C_3N_4 because the VB edge potential of TiO_2 (2.91 eV) is more positive than that of g-C_3N_4 (1.4 eV). In this case, photoinduced electrons accumulate in the CB of TiO_2 for the reduction reaction and photoinduced holes accumulate in the VB of g-C_3N_4 for the oxidation reaction, which efficiently separates the photogenerated electron–hole pairs and suppresses their recombination [102–104]. However, despite the enhanced photocatalytic efficiency of the as-constructed TiO_2/g-C_3N_4 nanocomposite, a drawback of the Type-II heterojunction mechanism is attributed to the impairment of redox capability, since the reduction reaction proceeds on TiO_2 with a lower reduction potential compared with g-C_3N_4, and the oxidation reaction proceeds on g-C_3N_4 with a lower oxidation potential compared with TiO_2 [102,103]. Since the holes in the VB of g-C_3N_4 cannot directly generate

OH radicals in the oxidation reaction, this significantly reduces the photocatalytic efficiency of the nanocomposite.

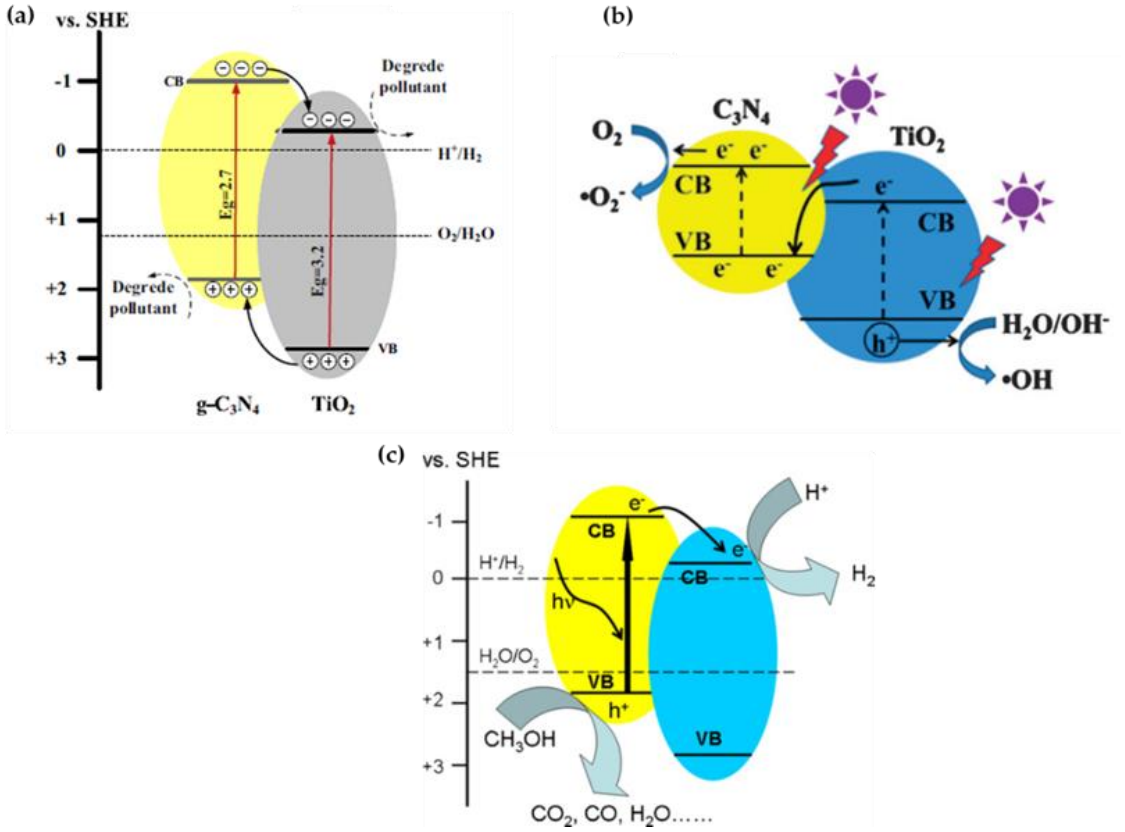

Figure 6. The photocatalytic mechanism of the TiO_2/g-C_3N_4 heterojunction: Type II (**a**) (reprinted with permission from [82]; Copyright 2012, Elsevier), and Z-scheme (**b**) (reprinted with permission from [91]; Copyright 2013, RSC Publishing) under UV/visible light irradiation; electron transfer pathway under exclusive visible light irradiation (**c**). Reprinted with permission from [81]; Copyright 2011, Elsevier.

In contrast to the Type-II heterojunction mechanism, the direct Z-scheme photocatalysis system assumes a significantly different charge carrier transfer pathway in the TiO_2/g-C_3N_4 nanocomposite, although it has the same band structure configuration (Figure 6b) [102]. Indeed, the direct Z-scheme dictates that the existence of an internal electric field, the extra potential barrier, and the Coulomb repulsion hinder the transfer of the photogenerated electrons from the CB of g-C_3N_4 to the CB of TiO_2 and the photogenerated holes from the VB of TiO_2 to the VB of g-C_3N_4, as well as promoting the recombination between the photogenerated electrons in the CB of TiO_2 and the photogenerated holes in the VB of g-C_3N_4 with a lower redox ability [102,103]. In this case, the electrons and holes are spatially separated on g-C_3N_4 with the higher reduction potential and TiO_2 with a higher oxidation potential, respectively. The electrons in the CB of g-C_3N_4 are trapped by O_2 on the nanocomposite surface to form reactive $\bullet O_2^-$, since the CB edge potential of g-C_3N_4 (−1.3 eV) is more negative than the redox potential of $O_2/\bullet O_2^-$ (−0.33 eV and −0.046 eV), while the holes in VB of TiO_2 react with absorbed water to generate reactive •OH radicals [91] because the VB edge potential of TiO_2 (2.91 eV) is more positive than the redox potential of $^-$OH/•OH (+1.99 eV). Compared with the Type-II heterojunction, the direct Z-scheme has a much stronger redox capability to drive photocatalytic reactions [102], which could explain the superior photocatalytic efficiency of TiO_2/g-C_3N_4 nanocomposite in the various reduction and oxidation reactions. The presence of the direct Z-scheme

instead of the Type-II heterojunction was also confirmed by experiments involving the trapping of •OH and $\bullet O_2^-$ radicals [103].

On the other hand, when irradiated with visible light, when only g-C_3N_4 can be excited because the energy of the incident light is too low to excite TiO_2, the reduction reaction on the TiO_2 surface can be indirectly induced via electron transfer from the CB of g-C_3N_4 to the CB of TiO_2, leading to effective separation of photogenerated electron–hole pairs and an enhanced photocatalytic activity (Figure 6c) [81,84,96].

3.2. TiO_2/g-C_3N_4 Nanocomposites for Textile Application

TiO_2/g-C_3N_4 nanocomposites were applied to cotton and polyester substrates to develop textile-based photocatalysts for effective purification of emerging liquid, gaseous pollutants, and bacteria [39,105–107]. To this end, TiO_2/g-C_3N_4–cotton and TiO_2/g-C_3N_4–polyester composites were constructed and used as solar-driven photocatalysts for the degradation of the antibiotic sulphaquinoxaline (SQX) and the pesticide thiamethoxam (Figure 7) [106,107]. The preparation of a TiO_2@g-C_3N_4–cotton photocatalyst included binding of the coupling agent (3-Aminopropyl)triethoxysilane (APTES) to the carboxyl-modified g-C_3N_4, to create reactive silanol groups on the g-C_3N_4 surface. Afterwards, a cotton fabric sample was immersed in the g-C_3N_4–APTES hydrolysate, followed by squeezing on a two-roll padder and drying at 130 °C, to chemically bind g-C_3N_4–APTES to the cotton surface. To produce the TiO_2@g-C_3N_4–cotton, a g-C_3N_4–APTES-cotton sample was immersed in the TiO_2 dispersion and maintained at 120 °C for 2 h for hydrothermal reaction, to achieve the deposition of TiO_2 on the g-C_3N_4–APTES-cotton surface (Figure 7a). In the preparation of the g-C_3N_4-TiO_2@LMPET photocatalyst, low-melting non-woven polyester (LMPET) was immersed in the g-C_3N_4 dispersion, followed by squeezing and drying at 80 °C, and heat treated at 135 °C, to melt the LMPET sheath to strongly stick g-C_3N_4. The as-prepared g-C_3N_4@LMPET was immersed in the TiO_2 dispersion and maintained at 120 °C for 2 h for hydrothermal reaction, to achieve the deposition of TiO_2 on the g-C_3N_4@LMPET surface (Figure 7b).

The incorporation of the TiO_2/g-C_3N_4 nanocomposite into the cotton and LMPET significantly changed the morphology of the fibers, resulting in an increased surface roughness of the cotton (Figure 8a–d) [107] as well as LMPET [106]. Photocatalytic activity was studied in the degradation of the antibiotic sulphaquinoxaline (SQX) (Figure 8e,f) and the pesticide thiamethoxam (Figure 8g,h) under sunlight irradiation. It was found that both the TiO_2@g-C_3N_4-cotton and g-C_3N_4-TiO_2@LMPET samples showed excellent photocatalytic performance, resulting in an almost 100% degradation of SQX after 60 and 90 min by the TiO_2@g-C_3N_4-cotton and g-C_3N_4-TiO_2@LMPET samples, respectively, and of thiamethoxam after 150 and 180 min by TiO_2@g-C_3N_4-cotton and g-C_3N_4-TiO_2@LMPET samples, respectively, at pH 7. The photocatalytic performance was sufficiently higher than that of the TiO_2-cotton and TiO_2@LMPET samples and that of the g-C_3N_4-cotton and g-C_3N_4@LMPET samples. The rate of SQX removal by TiO_2/g-C_3N_4 was higher than that of thiamethoxam for both textile-based photocatalysts, because thiamethoxazine is a more difficult pollutant to degrade than SQX. The results also showed that the TiO_2/g-C_3N_4 composite exhibited better photocatalytic activity in the decomposition of SQX under acidic and neutral conditions and gradually weakened under alkaline conditions (Figure 8i). Both TiO_2@g-C_3N_4-cotton and g-C_3N_4-TiO_2@LMPET photocatalysts maintained excellent catalyst recyclability and stability and could remove 97% SQX after 10 cycles.

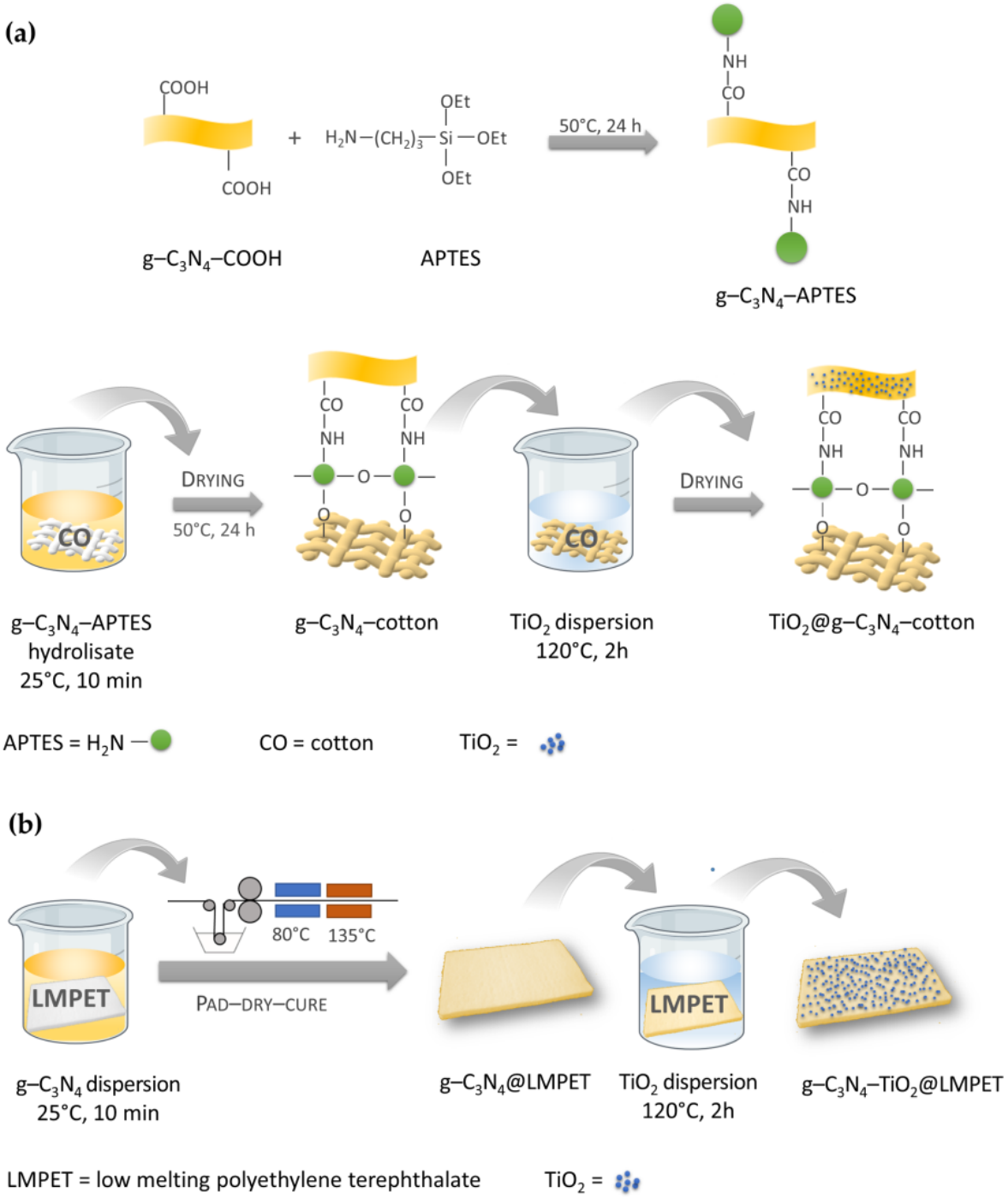

Figure 7. Schematic presentation of the preparation of the TiO_2@g-C_3N_4–cotton (**a**) and the g-C_3N_4-TiO_2@LMPET (**b**) photocatalysts (prepared according to refs. [106,107].

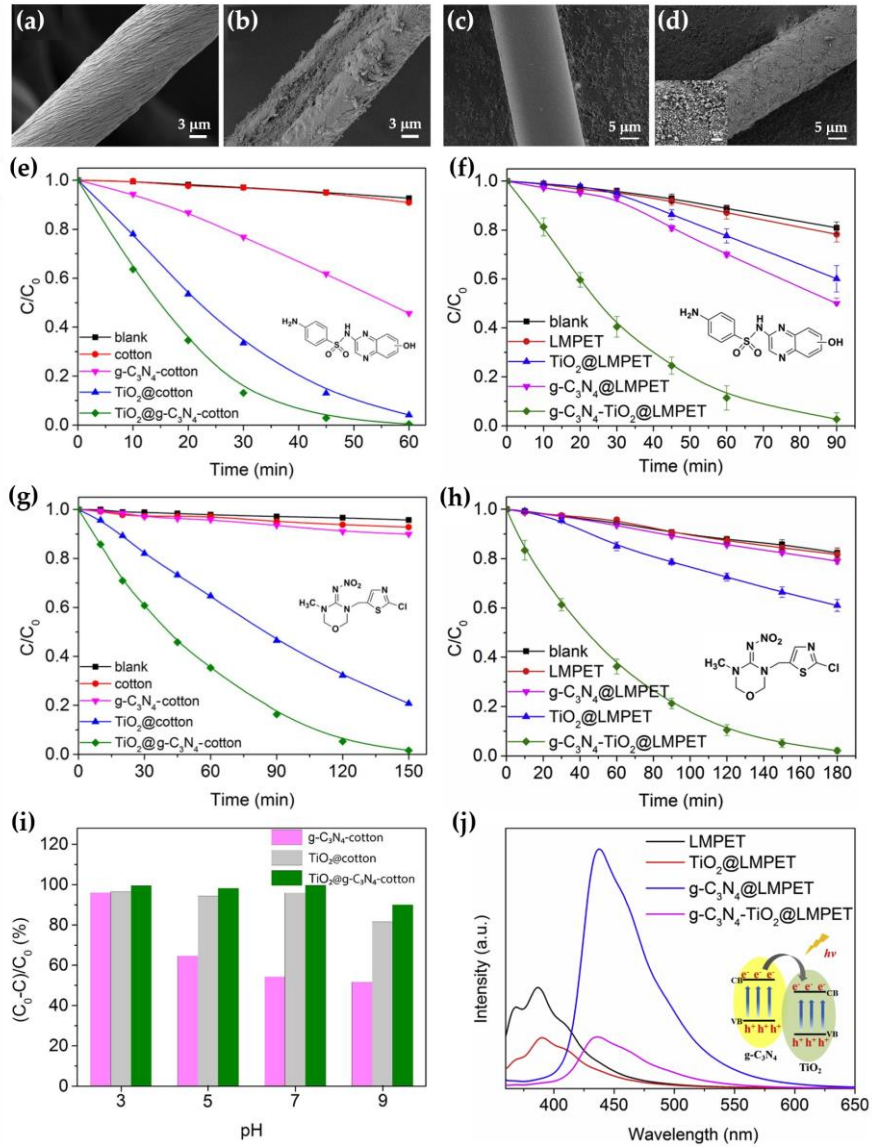

Figure 8. SEM images of cotton (**a**), TiO_2@g-C_3N_4–cotton (**b**), LMPET (**c**), and g-C_3N_4-TiO_2@LMPET (**d**) samples; photocatalytic degradation of SQX by cotton-based photocatalysts (**e**) and LMPET-based photocatalysts (**f**) under solar irradiation, [SQX] = 2×10^{-5} mol/L, pH 7; photocatalytic degradation of thiamethoxam by cotton-based photocatalysts (**g**), and LMPET-based photocatalysts (**h**) under solar irradiation, [thiamethoxam] = 2×10^{-5} mol/L, pH 7; photocatalytic degradation rate of SQX by cotton-based photocatalysts at different pH under solar irradiation for 60 min, [SQX] = 2×10^{-5} mol/L (**i**); photoluminescence spectra of LMPET and LMPET-based photocatalysts (**j**). (**a**,**b**,**e**,**g**,**i**) Reprinted with permission from [107]; Copyright 2021, Elsevier; (**c**,**d**,**f**,**h**,**j**) Reprinted with permission from [106], Copyright 2019, Elsevier.

The mechanism of the photocatalytic activity of the TiO_2/g-C_3N_4 heterojunction and the behavior of the charge transfer at the interface were discussed based on the photoluminescence spectra (Figure 8j) [106]. The results showed that g-C_3N_4 exhibited a strong emission peak at about 450 nm, which decreased drastically in the case of the TiO_2/g-C_3N_4 heterojunction. This phenomenon can be explained by the electron transfer from the CB of g-C_3N_4 to the CB of TiO_2, which efficiently suppresses the recombination of photogenerated electron–hole pairs and improves the photocatalytic performance compared with the single-components TiO_2 and g-C_3N_4, indicating a synergistic effect between TiO_2 and g-C_3N_4 in the heterojunction.

A textile-based photocatalyst was also prepared by constructing a TiO_2/g-C_3N_4 coating on cotton fabric using a simple layer-by-layer (LBL) self-assembly strategy, in which the cotton fabric was alternately immersed in the cationic TiO_2 solution and the anionic g-C_3N_4 solution to obtain two, five, and seven bilayers (BL) [105]. After each immersion, the sample was rinsed and dried. A TiO_2/g-C_3N_4 powder composite was also prepared for comparison. The SEM analysis revealed that the self-assembly coating mainly covered the surface of the cotton fibers and significantly increased their roughness (Figure 9a). The mass of the coating increased with the number of BL. The photocatalytic performance of the TiO_2/g-C_3N_4 coated cotton fabric was investigated through the degradation rate of RhB dye (Figure 9b) and toluene (Figure 9c) under visible-light irradiation. The higher the degradation rate constant, the higher the photocatalytic performance. From the results, it can be seen that the reaction rate constant, κ, for the degradation of Rhodamine B (RhB) dye gradually increased with the increasing number of BL, and the highest value was reached for the coating with 7 BL, which was much higher than that of TiO_2/g-C_3N_4 and TiO_2 powders (Figure 9b). This confirmed that the coupling of TiO_2 with g-C_3N_4 is an efficient strategy to improve photocatalytic performance and highlights the importance of the cotton fabric as a support for the photodegradation reaction, since the fabric acts as an absorbent for pollution and drives the active species to rapidly absorb and degrade the pollutants. Similar results were obtained for the photodegradation of toluene, with coatings of 2 BL, 5 BL, and 7 BL showing significantly higher degradation compared with the TiO_2/g-C_3N_4 powder (Figure 9c). The excellent performance of the 7 BL coated cotton fabric was also demonstrated by the degradation of RhB solution under sunlight, where not only was the RhB solution completely discolored within 4 h but also the coated fabric, indicating RhB degradation in the solution and on the fabric surface (Figure 9d).

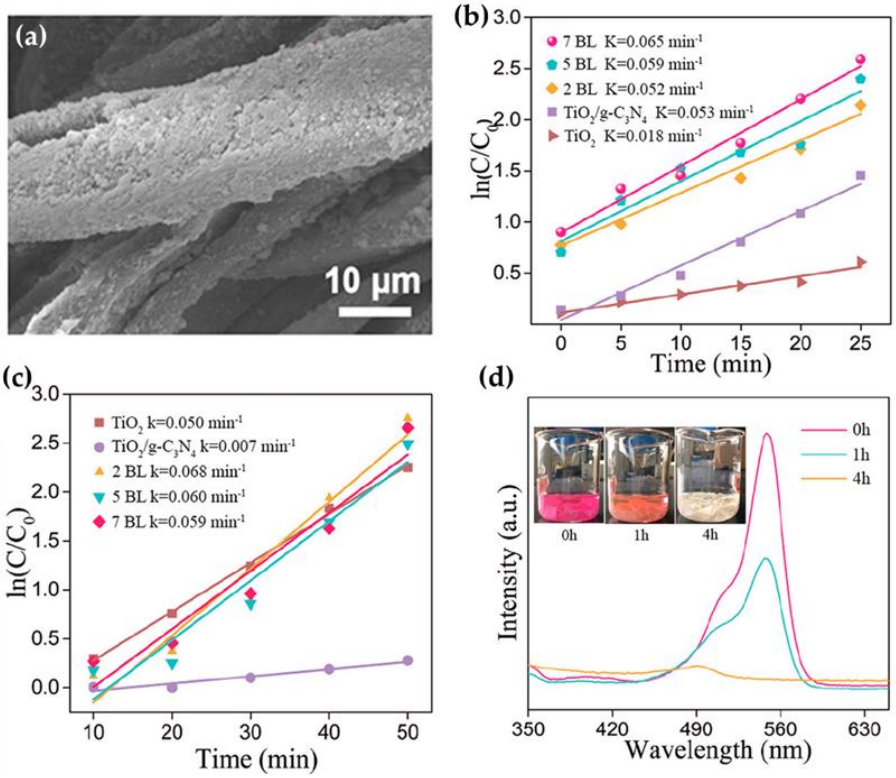

Figure 9. SEM images of the cotton modified with TiO_2/g-C_3N_4 (**a**); kinetic degradation curves of RhB under visible-light irradiation (**b**), kinetic degradation curves of toluene under simulated sunlight irradiation (**c**); absorption spectra of RhB under real sunlight (**d**). Reprinted with permission from [105]. Copyright 2019, ACS Publications.

To investigate the photocatalytic mechanism, a TiO_2/g-C_3N_4 nanocomposite was chemically grafted onto cotton fibers in a hydrothermal process (Figure 10) [39]. In the preparation of cotton fabric loaded with TiO_2/g-C_3N_4 in different mass ratios (C–g-C_3N_4–TiO_2 samples), the in situ synthesis of TiO_2 was performed in a solution of presynthesized g-C_3N_4 nanosheets in the presence of the swollen cotton fibers at 120 °C for 4 h. The results showed that the as-prepared C–g-C_3N_4–TiO_2 samples exhibited fish-like lobes, with densely aggregated nanosized particles of irregular shape (Figure 10a). Chemical grafting of the g-C_3N_4–TiO_2 heterojunction composite with cotton fibers resulted in an Eg of 3.31 eV, which was red-shifted compared with the Eg of C–TiO_2 fibers of 3.45 eV (Figure 10b), indicating a higher light absorption efficiency. Both calculated Eg values were higher than those of TiO_2 NPs (Eg = 3.2 eV) and g-C_3N_4 nanosheets (Eg = 2.82 eV), suggesting that cotton affected the energy band structure of the generated composite photocatalysts, which is difficult to explain.

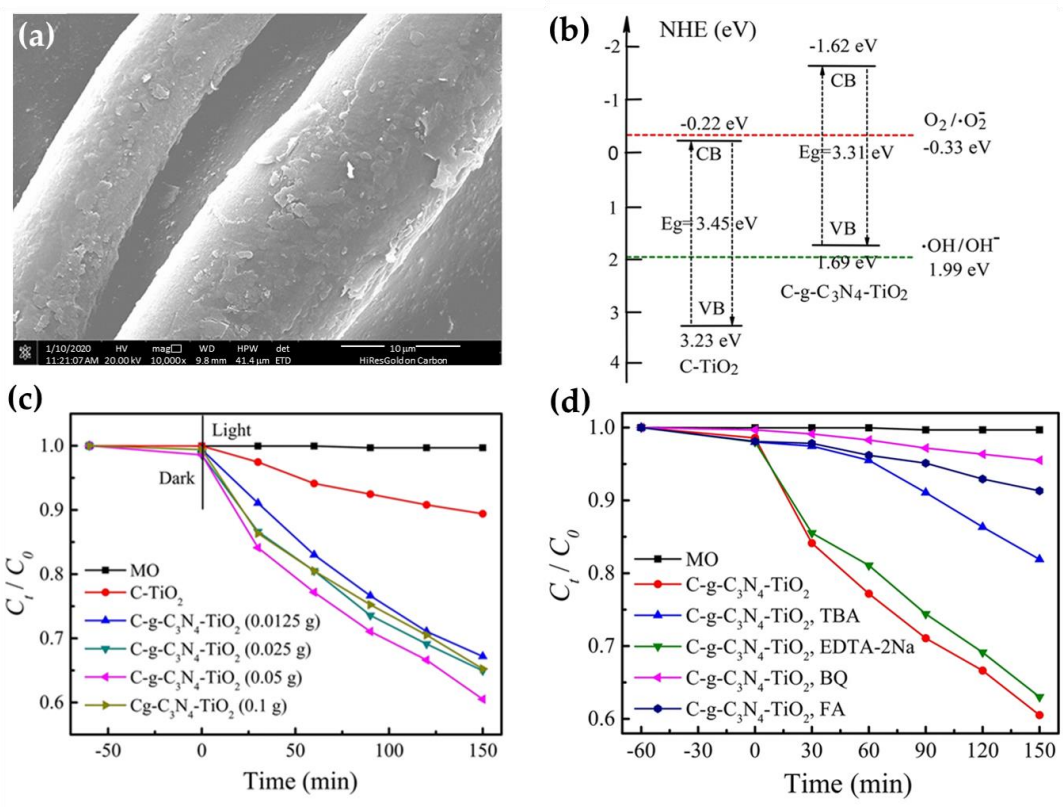

Figure 10. FESEM images of C–g-C_3N_4–TiO_2 cotton fibers (**a**); schematic diagrams of energy band structure for C–TiO_2 and C–g-C_3N_4–TiO_2 cotton fibers (**b**); photodegradation of MO dye solution by the C–g-C_3N_4–TiO_2 cotton fibers (**c**); trapping experiments for the photodegradation of MO dye solution by C–g-C_3N_4–TiO_2 cotton fibers (**d**). Reprinted with permission from [39]. Copyright 2021, Springer Link.

The photocatalytic performance results of the C–g-C_3N_4–TiO_2 and C–TiO_2 samples showed that the C–TiO_2 cotton fibers exhibited a poor photodegradation performance for methyl orange (MO) dye solution when irradiated with visible light, with only 10% MO decolorization after 150 min, while the photocatalytic performance of the C–g-C_3N_4–TiO_2 cotton fibers was much higher (Figure 10c) [39]. The latter increased with the increase in the mass of the g-C_3N_4 nanosheets in the TiO_2/g-C_3N_4 nanocomposite, from 0.025 to 0.05 g, and reached its maximum with a photocatalytic efficiency about four-times higher than that of the C–TiO_2 cotton fibers. Further increasing the mass of the g-C_3N_4 nanosheets led to a decrease in the photocatalytic activity of the C–g-C_3N_4–TiO_2 cotton fibers, indicating that the mass ratio between g-C_3N_4 and TiO_2 in the heterojunction should be carefully selected.

The photocatalytic mechanism of action of the C–g-C_3N_4–TiO_2 cotton fibers was determined through trapping experiments (Figure 10d) [39], in which photodegradation of the MO dye solution was performed under irradiation with visible light in the presence of four radical scavengers, i.e., 1,4-benzoquinone (BQ), furfuryl alcohol (FA), tertbutyl alcohol (TBA), and ethylenediaminetetraacetic acid disodium salt (EDTA-2Na) to scavenge $\bullet O_2^-$, singlet oxygen ($^1O_2$), •OH and h^+, respectively. It was found that the photocatalytic activity of the C–g-C_3N_4–TiO_2 cotton fibers decreased only slightly in the presence of EDTA-2Na, but a significant decrease in photocatalytic capacity was observed after the addition of BQ and FA. This indicates that $\bullet O_2^-$, generated by the reduction reaction at the surface of the TiO_2/g-C_3N_4 heterojunction, is the most important type of radical for the photocatalytic degradation of MO, followed by $^1O_2$, •OH, and h^+. It was concluded that cotton fabric modified with g-C_3N_4–TiO_2 can be repeatedly used to remove organic contaminants.

4. Ag/TiO_2/g-C_3N_4 Heterostructure

Preparation and Photocatalytic Mechanism of Ag/TiO_2/g-C_3N_4 Nanocomposites

The construction of ternary Ag/TiO_2/g-C_3N_4 heterostructures represents a very promising strategy for achieving the enhanced photocatalytic performance of semiconductor nanocomposites under visible light irradiation [43,45,108–126]. Various approaches for the synthesis of Ag/TiO_2/g-C_3N_4 nanocomposites have been reported in the literature. One of these proposes the preparation of a mixture of Ag, TiO_2 and g-C_3N_4 precursors and the synthesis of an Ag/TiO_2/melamine nanocomposite at 70 °C, followed by calcination of the nanocomposite at 550 °C, to produce g-C_3N_4 from melamine (Figure 11a) [126]. Another strategy is to mix previously synthesized TiO_2 and g-C_3N_4, followed by the addition of an $AgNO_3$ precursor and synthesis of Ag NPs in the presence of a g-C_3N_4 and TiO_2 mixture or previously prepared TiO_2/g-C_3N_4 nanocomposite (Figure 11b1,b2) [45,115,123,124]. A TiO_2/g-C_3N_4 composite was also prepared by the synthesis of g-C_3N_4 from a suitable precursor in the presence of TiO_2 or through the synthesis of TiO_2 from a suitable precursor in the presence of g-C_3N_4, followed by the synthesis of Ag NPs from an $AgNO_3$ precursor in a reduction reaction in the presence of TiO_2/g-C_3N_4 nanocomposite (Figure 11c1,c2) [108,116,117]. It has also been reported that the Ag/TiO_2/g-C_3N_4 nanocomposite was prepared by synthesis of Ag NPs from an $AgNO_3$ precursor in the presence of TiO_2 and subsequent mixing of the Ag/TiO_2 nanocomposite with previously synthesized g-C_3N_4 (Figure 11d) [43,110,113,118,119,121,122].

It should be emphasized that the photocatalytic mechanism of the ternary Ag/TiO_2/g-C_3N_4 nanocomposite is very complex and not yet fully understood. Since it is influenced by nanocomposite construction, which is directly related to the synthesis route and the formation of tight interfacial connections between the components in the heterojunction, there are various schematic representations of the photocatalytic mechanisms of Ag/TiO_2/g-C_3N_4 in the literature, as well as explanations of the charge carrier transfer. The most commonly proposed mechanisms are shown in Figure 12 [45,116,120,122].

It is proposed that the enhanced photocatalytic performance of Ag/TiO_2/g-C_3N_4 is due to the effective Z-scheme mechanism established in the TiO_2 and g-C_3N_4 heterojunction under UV- and visible-light irradiation, which is supported by the SPR of Ag facilitating charge transfer (Figure 12a) [45,108]. It has been suggested that Ag, as a conductive material, can directly act as a center to combine electrons on the surface of TiO_2 with the holes on g-C_3N_4 and maintain this remarkable Z-scheme photocatalytic system [45].

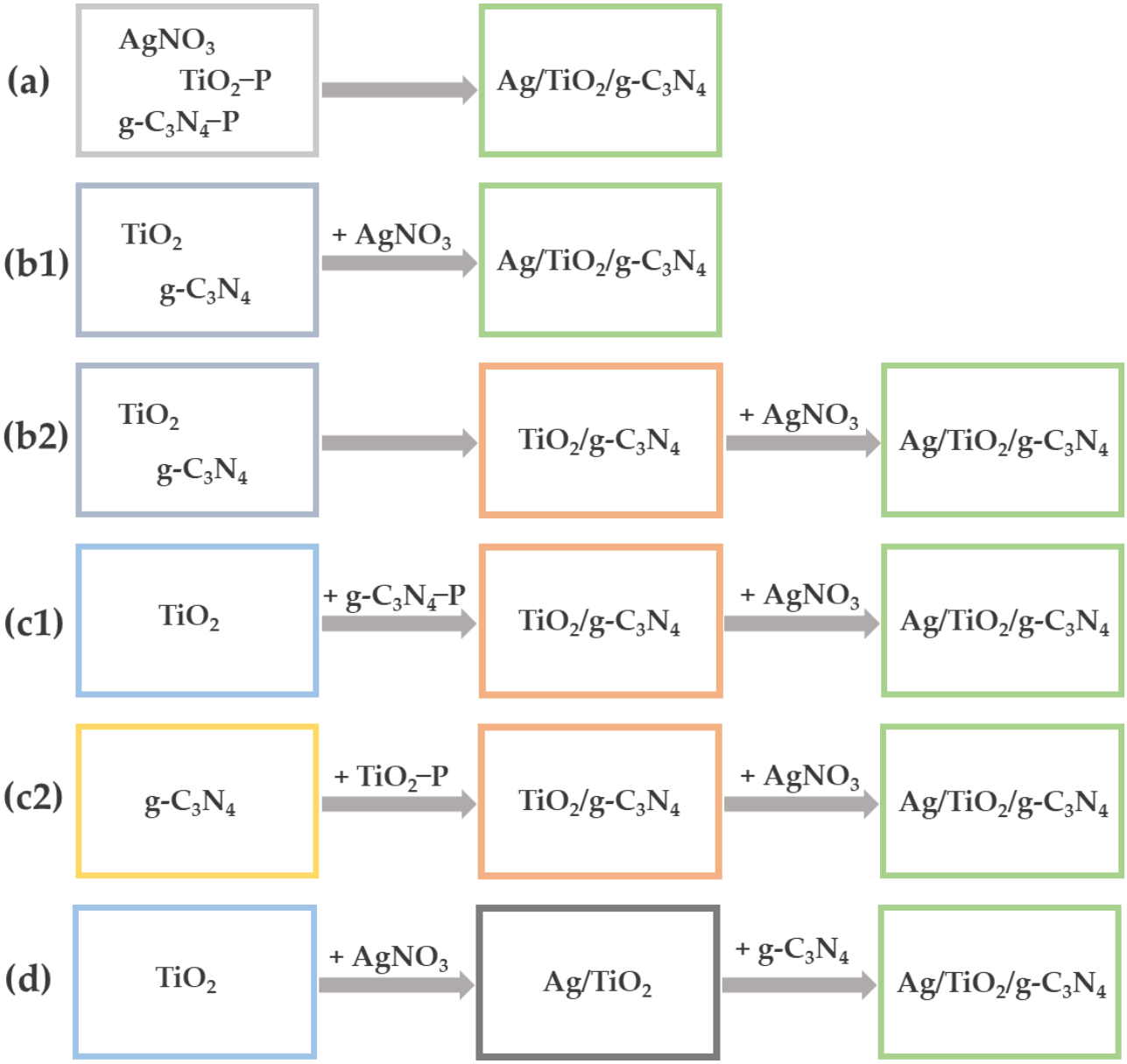

Figure 11. Schematic presentation of strategies for the synthesis of the $Ag/TiO_2/g\text{-}C_3N_4$ nanocomposites: synthesis of Ag/TiO_2/melamine from a mixture of Ag, TiO_2 and $g\text{-}C_3N_4$ precursors, followed by calcination to produce $Ag/TiO_2/g\text{-}C_3N_4$ (**a**); preparation of a mixture of TiO_2 and $g\text{-}C_3N_4$, followed by synthesis of Ag NPs (**b1**); synthesis of $TiO_2/g\text{-}C_3N_4$, followed by synthesis of Ag NPs (**b2**); synthesis of $g\text{-}C_3N_4$ in the presence of TiO_2, followed by the synthesis of Ag NPs (**c1**); synthesis of TiO_2 in the presence of $g\text{-}C_3N_4$, followed by the synthesis of Ag NPs (**c2**); synthesis of Ag NPs in the presence of TiO_2, followed by a mixture with $g\text{-}C_3N_4$ (**d**). P = precursor.

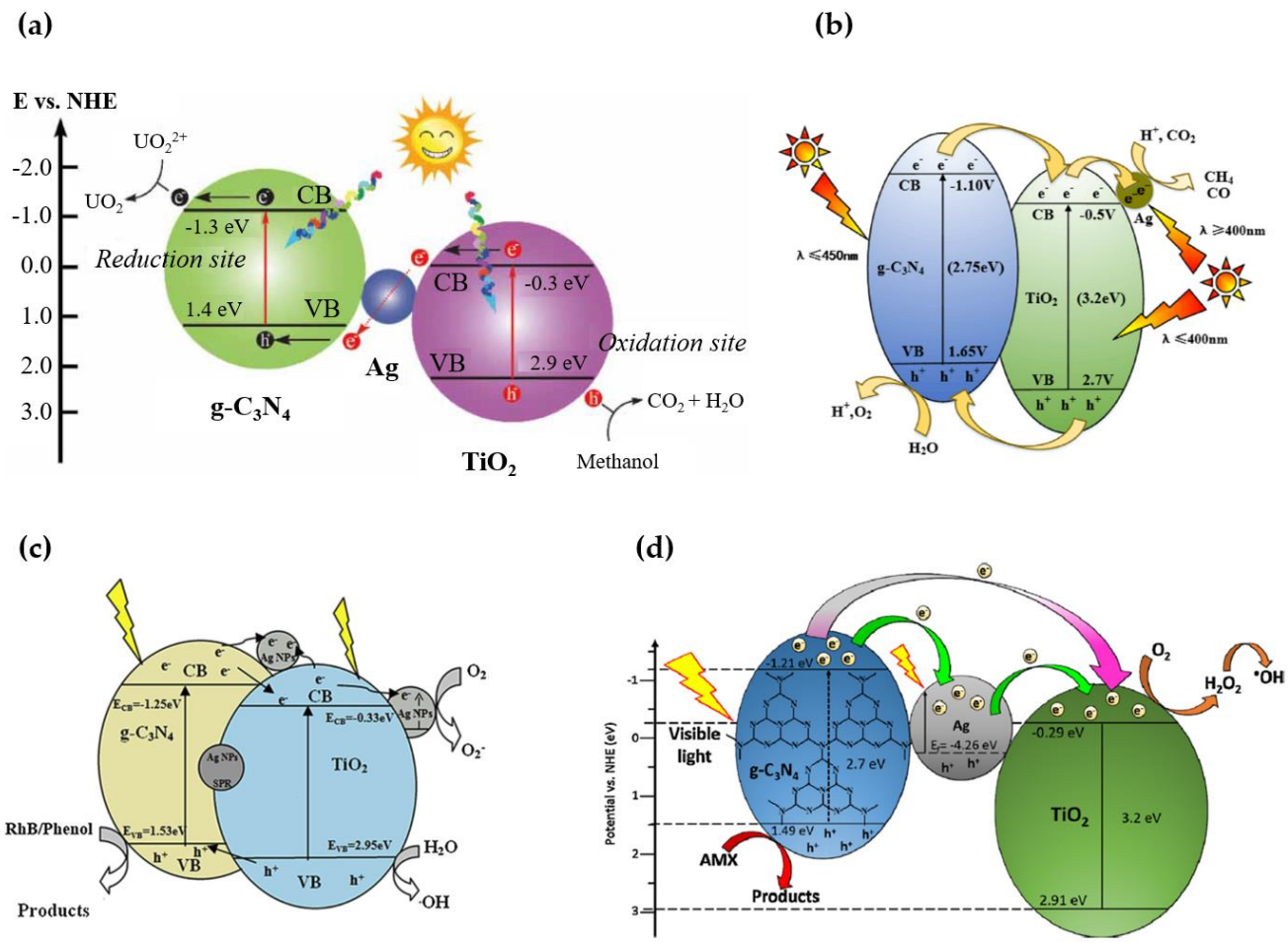

Figure 12. Direct Z-scheme of the photocatalytic mechanism of $Ag/TiO_2/g\text{-}C_3N_4$ heterostructure (**a**) (Reprinted with permission from [45]; Copyright 2022, IWA Publishing); Type II heterojunction of $Ag/TiO_2/g\text{-}C_3N_4$ accompanied by the Schottky barrier (**b**) (Reprinted with permission from [122]; Copyright 2017, Elsevier) and (**c**) (Reprinted with permission from [116], Copyright 2020, Elsevier); photocatalytic mechanism of $Ag/TiO_2/g\text{-}C_3N_4$ under visible light (**d**) (Reprinted with permission from [120], Copyright 2015, Elsevier).

Another possible photocatalytic mechanism of $Ag/TiO_2/g\text{-}C_3N_4$ involves the Type-II mechanism of the $TiO_2/g\text{-}C_3N_4$ heterojunction and Schottky barrier formed at the interfaces of Ag/TiO_2, Ag/gC_3N_4 or $TiO_2/Ag/g\text{-}C_3N_4$ (Figure 12b,c) [116,117,122,125,126]. According to this mechanism, both TiO_2 and $g\text{-}C_3N_4$ are excited under spectrum solar irradiation, but $g\text{-}C_3N_4$ mainly absorbs visible light and TiO_2 absorbs UV light. After excitation, photogenerated e^- can easily be transferred from the more negative CB of $g\text{-}C_3N_4$ to the less negative CB of TiO_2 and, at the same time, h^+ can be easily transferred from the more positive VB of TiO_2 to the less positive VB of $g\text{-}C_3N_4$ (Type-II mechanism). When Ag is deposited on TiO_2 in $TiO_2/g\text{-}C_3N_4$, e^- can be transferred from the CB of TiO_2 and trapped by Ag due to the Schottky barrier formed at the interface of the Ag and TiO_2 (Figure 12b) [117,121,122,124,126]. This promotes the separation of charge carriers and significantly enhances the photocatalytic activity. On the other hand, when Ag is deposited on TiO_2 and $g\text{-}C_3N_4$ in the ternary heterostructure, Ag captures the electrons from both $g\text{-}C_3N_4$ and TiO_2 (Figure 12c) [116,117,125]. The effect of the position of the noble metal in $TiO_2/g\text{-}C_3N_4$ on the photocatalytic activity was systematically investigated for ternary $Pt/TiO_2/g\text{-}C_3N_4$ nanocomposites, and the results showed that the efficiency increased as follows: Pt deposited only on $g\text{-}C_3N_4$ < Pt deposited on both TiO_2 and $g\text{-}C_3N_4$ < Pt deposited only on TiO_2 [127].

In some of the reported studies, only visible light was used as the excitation source, and it was suggested that only g-C_3N_4 absorbs the visible light photons and is excited [118,120,128]. Subsequently, the photogenerated e^- in the CB of g-C_3N_4 can be transferred to the CB of TiO_2. It has been suggested that the Ag deposited on the surface of TiO_2 plays a key role as an electron conduction bridge, to transfer the electron from the CB of g-C_3N_4 to the CB of TiO_2. The formation of a Schottky barrier at the interface between Ag and TiO_2 efficiently enhances the electron transfer to TiO_2 and the separation of electron−holes in g-C_3N_4 [118,120]. At the same time, the SPR effect of Ag contributes significantly to the absorption of visible light in the Ag/TiO_2/g-C_3N_4 nanocomposite. However, it is also believed that the strong electron oscillation in the SPR in Ag under visible light triggers the transfer of energetic electrons from Ag into the TiO_2 conduction band, thus shattering the Schottky barrier (Figure 12d) [120]. It is hypothesized that loading of TiO_2 with Ag can cause the shift of the Fermi level of Ag to a more negative level and of TiO_2 to a more positive level, to achieve a new Fermi level equilibrium that allows the transfer of the energetic plasmon electrons of Ag NPs across the energy barrier into the conduction band of TiO_2 [115]. In this case, the oxidation reaction occurs at the surface of TiO_2, while the holes of g-C_3N_4 are directly involved in the oxidation reaction.

In the literature, an Ag/TiO_2/g-C_3N_4 ternary nanocomposite has not yet been applied to textile fibers, although it has been established as a powerful nanomaterial for the photocatalytic degradation of various dyes [43,108,113,116,118,121,123,124], phenol [118], acetaldehyde [119], formaldehyde [117], ammonia [109], and carbon dioxide [122]; hard metals, such as hexavalent chromium [108,109]; and uranium from uranium-containing wastewater [45]. Ag/TiO_2/g-C_3N_4 nanocomposite has already been used for photocatalytic hydrogen evolution [115,126], solar water oxidation [112], electron transport in organic solar cells [114], vitamin B3 production [110], and as an antibacterial agent [108,111]. Due to its excellent multifunctional properties, the use of Ag/TiO_2/g-C_3N_4 nanocomposite for the chemical modification of textile fibers is still a promising research challenge.

5. Conclusions and Future Perspectives

In this review, binary Ag/g-C_3N_4 and TiO_2/g-C_3N_4 nanostructures and ternary Ag/TiO_2/g-C_3N_4 nanostructure were presented as very promising and effective nanocomposites with Schottky, Type II, and Z-scheme mechanisms of photocatalysts. All the above nanocomposites have attracted much attention, due to their ability to initiate and carry out various reduction and oxidation reactions under visible light, and can thus be advantageous when used in environmental remediation, energy storage and conversion, sustainable catalysis, biosensing, and antimicrobial disinfection.

For textile applications, binary Ag/g-C_3N_4 and TiO_2/g-C_3N_4 composites have emerged as promising functional nanomaterials, because the synergistic effect of the components in the heterostructures leads to improved photocatalytic performance of the composites compared with the single-component material itself. The Ag/g-C_3N_4 nanocomposites not only exhibit enhanced visible-light photocatalytic performance but also an improved antimicrobial performance, due to the excellent antimicrobial activity of Ag. In the preparation of Ag/g-C_3N_4 nanocomposites, g-C_3N_4 is surface-decorated with Ag during the in situ synthesis of Ag^0 from $AgNO_3$ precursor in the suspension of presynthesized g-C_3N_4. Another approach is to mix urea, melamine, and/or cyanuric acid with $AgNO_3$ precursors and then synthesize Ag-doped g-C_3N_4 under suitable conditions. Compared to bare g-C_3N_4, it is believed that the efficiency of the Ag/g-C_3N_4 nanocomposite is significantly enhanced by the presence of Ag^0, which acts as a current collector and plasmonic absorber. The Schottky barrier formed at the interface between Ag and g-C_3N_4 maximizes photoinduced charge carrier separation and prevents electron–hole pair recombination. The nanocomposite photoactivity is further enhanced by plasmon resonance energy transfer, as the intense electric near field induced by SPR improves the efficiency of charge carrier separation. The exceptional photocatalytic performance of Ag/g-C_3N_4 nanocomposites on

textile substrates has already been advantageously used for the photochemical activation of organic syntheses and as a textile-based source for wearable electronics.

The two-semiconductor heterojunction of TiO_2 and g-C_3N_4 has been recognized as an effective material for various environmental and energy applications. TiO_2/g-C_3N_4 was prepared by various synthetic routes, including the facile mixing of prepared TiO_2 and g-C_3N_4 under suitable conditions, the in situ synthesis of TiO_2 from its precursor in the presence of presynthesized g-C_3N_4, or conversely, the in situ synthesis of g-C_3N_4 from its precursor in the presence of presynthesized TiO_2. Moreover, the precursors of TiO_2 and g-C_3N_4 were simultaneously mixed in sol to synthesize the TiO_2/g-C_3N_4 heterojunction. An important step in the synthesis process is the calcination of the nanocomposites under suitable conditions, to obtain the desired morphology of the nanocomposite. The unique properties of the TiO_2/g-C_3N_4 heterojunction are related to the simultaneous utilization of UV and visible light, resulting in excellent photocatalytic performance under UV- and visible-light irradiation. When TiO_2/g-C_3N_4 is excited by incident UV/visible light of sufficient energy, the Type-II heterojunction and the direct Z-scheme charge carrier transfer pathway are adopted in the photocatalytic mechanism of the TiO_2/g-C_3N_4 nanocomposite. According to the band edge potentials, the Type-II heterojunction allows the transfer of the photogenerated electrons from the CB of g-C_3N_4 to the CB of TiO_2 and the photogenerated holes from the VB of TiO_2 to the VB of g-C_3N_4. This causes the reduction reaction on TiO_2 to proceed with a lower reduction potential compared with g-C_3N_4, and the oxidation reaction on g-C_3N_4 to proceed with a lower oxidation potential compared to TiO_2, which is a disadvantage of the Type-II heterojunction mechanism. On the other hand, despite having the same band structure configuration, the direct Z-scheme assumes a much stronger redox capability for the TiO_2/g-C_3N_4 heterojunction because it promotes the spatial separation of electrons and holes on g-C_3N_4 with the higher reduction potential and on TiO_2 with the higher oxidation potential, respectively, and promotes the recombination between the photogenerated electrons in the CB of TiO_2 and the photogenerated holes in the VB of g-C_3N_4 with the lower redox capability. The superior photocatalytic efficiency of TiO_2/g-C_3N_4 nanocomposite has already been beneficially utilized in the development of textile-based photocatalysts for the effective purification of liquid and gaseous pollutants and bacteria.

There is no evidence in the literature that an Ag/TiO_2/g-C_3N_4 ternary nanocomposite has been used for textile applications, although it is a promising strategy for the surface- and bulk-modification of textiles. There are many strategies to prepare Ag/TiO_2/g-C_3N_4 heterostructures, including simultaneous synthesis of the nanocomposite from suitable precursors, in situ synthesis of Ag in the presence of a previously synthesized TiO_2/g-C_3N_4 composite, and surface decoration of TiO_2 by Ag and subsequent mixing with g-C_3N_4. The synthesis pathway directly affects the photocatalytic mechanism of the Ag/TiO_2/g-C_3N_4 nanocomposite, which can be explained by the direct Z-scheme or the Type-II mechanisms established in the TiO_2 and g-C_3N_4 heterojunction, supported by the Schottky barrier and SPR of Ag. The great potential of the Ag/TiO_2/g-C_3N_4 ternary nanocomposite lies in its ability to provide multifunctional textile properties, such as photocatalytic self-cleaning, antimicrobial activity, UV protection, conductivity, and thermal stability. Therefore, the development of textile platforms with integrated Ag/TiO_2/g-C_3N_4 heterostructures is a major challenge, where the in situ synthesis of Ag/TiO_2/g-C_3N_4 in the presence of textile fibers as an stabilizing agent is a priority. Due to the additional requirements imposed on textile materials, the preparation of simultaneously effective, multifunctional, non-cytotoxic, and durable chemical modification of textile substrates will certainly be a hot research topic and will open new application opportunities for textile-based Ag/TiO_2/g-C_3N_4 nanocomposites.

Author Contributions: Conceptualization, B.S. and D.G.; writing—original draft preparation, B.S. and D.G.; review and editing, B.T., I.J., D.G., and R.S.C.; review, editing, and funding acquisition, B.S. All authors have read and agreed to the published version of the manuscript.

Funding: This research was funded by the Slovenian Research Agency, Slovenia (Programme P2-0213 Textiles and Ecology, Programme P1-0143 Circulation of substances in the environment, material balance and modeling of environmental processes and risk assessment, Infrastructural Centre RIC UL-NTF, BI-US/22-24-162, and a Grant for the doctoral student D.G.).

Data Availability Statement: The data presented in this study are available on request from the corresponding author.

Conflicts of Interest: The authors declare no conflict of interest.

References

1. Mamba, G.; Mishra, A.K. Graphitic carbon nitride (g-C_3N_4) nanocomposites: A new and exciting generation of visible light driven photocatalysts for environmental pollution remediation. *Appl. Catal. B Environ.* **2016**, *198*, 347–377. [CrossRef]
2. Sudhaik, A.; Raizada, P.; Shandilya, P.; Jeong, D.Y.; Lim, J.H.; Singh, P. Review on fabrication of graphitic carbon nitride based efficient nanocomposites for photodegradation of aqueous phase organic pollutants. *J. Ind. Eng. Chem.* **2018**, *67*, 28–51. [CrossRef]
3. Wang, J.; Wang, S. A critical review on graphitic carbon nitride (g-C_3N_4)-based materials: Preparation, modification and environmental application. *Coord. Chem. Rev.* **2022**, *453*, 214338. [CrossRef]
4. Hao, Q.; Jia, G.; Wei, W.; Vinu, A.; Wang, Y.; Arandiyan, H.; Ni, B.J. Graphitic carbon nitride with different dimensionalities for energy and environmental applications. *Nano Res.* **2020**, *13*, 18–37. [CrossRef]
5. Ashritha, M.G.; Hareesh, K. A review on Graphitic Carbon Nitride based binary nanocomposites as supercapacitors. *J. Energy Storage* **2020**, *32*, 101840. [CrossRef]
6. Ratshiedana, R.; Kuvarega, A.T.; Mishra, A.K. Titanium dioxide and graphitic carbon nitride–based nanocomposites and nanofibres for the degradation of organic pollutants in water: A review. *Environ. Sci. Pollut. Res.* **2021**, *28*, 10357–10374. [CrossRef]
7. Chouhan, R.S.; Jerman, I.; Heath, D.; Bohm, S.; Gandhi, S.; Sadhu, V.; Baker, S.; Horvat, M. Emerging tri-s-triazine-based graphitic carbon nitride: A potential signal-transducing nanostructured material for sensor applications. *Nano Sel.* **2021**, *2*, 712–743. [CrossRef]
8. Liang, Q.; Shao, B.; Tong, S.; Liu, Z.; Tang, L.; Liu, Y.; Cheng, M.; He, Q.; Wu, T.; Pan, Y.; et al. Recent advances of melamine self-assembled graphitic carbon nitride-based materials: Design, synthesis and application in energy and environment. *Chem. Eng. J.* **2021**, *405*, 126951. [CrossRef]
9. Shen, Y.; Dos Santos-Garcia, A.J.; de Vidales, M.J.M. Graphitic carbon nitride-based composite in advanced oxidation processes for aqueous organic pollutants removal: A review. *Processes* **2021**, *9*, 66. [CrossRef]
10. Tan, J.; Li, Z.; Li, J.; Wu, J.; Yao, X.; Zhang, T. Graphitic carbon nitride-based materials in activating persulfate for aqueous organic pollutants degradation: A review on materials design and mechanisms. *Chemosphere* **2021**, *262*, 127675. [CrossRef]
11. Guo, R.-t.; Wang, J.; Bi, Z.-x.; Chen, X.; Hu, X.; Pan, W.-g. Recent advances and perspectives of g–C_3N_4–based materials for photocatalytic dyes degradation. *Chemosphere* **2022**, *295*, 133834. [CrossRef]
12. Cao, S.W.; Yuan, Y.P.; Barber, J.; Loo, S.C.J.; Xue, C. Noble-metal-free g-C_3N_4/Ni(dmgH)$_2$ composite for efficient photocatalytic hydrogen evolution under visible light irradiation. *Appl. Surf. Sci.* **2014**, *319*, 344–349. [CrossRef]
13. Kang, Y.; Yang, Y.; Yin, L.C.; Kang, X.; Liu, G.; Cheng, H.M. An Amorphous Carbon Nitride Photocatalyst with Greatly Extended Visible-Light-Responsive Range for Photocatalytic Hydrogen Generation. *Adv. Mater.* **2015**, *27*, 4572–4577. [CrossRef]
14. Zhang, G.; Lan, Z.A.; Wang, X. Surface engineering of graphitic carbon nitride polymers with cocatalysts for photocatalytic overall water splitting. *Chem. Sci.* **2017**, *8*, 5261–5274. [CrossRef]
15. Lu, L.; Lv, Z.; Si, Y.; Liu, M.; Zhang, S. Recent progress on band and surface engineering of graphitic carbon nitride for artificial photosynthesis. *Appl. Surf. Sci.* **2018**, *462*, 693–712. [CrossRef]
16. Singla, S.; Sharma, S.; Basu, S.; Shetti, N.P.; Reddy, K.R. Graphene/graphitic carbon nitride-based ternary nanohybrids: Synthesis methods, properties, and applications for photocatalytic hydrogen production. *FlatChem* **2020**, *24*, 100200. [CrossRef]
17. Gkini, K.; Martinaiou, I.; Falaras, P. A review on emerging efficient and stable perovskite solar cells based on g-C_3N_4 nanostructures. *Materials* **2021**, *14*, 1679. [CrossRef]
18. Chen, L.; Song, J. Tailored Graphitic Carbon Nitride Nanostructures: Synthesis, Modification, and Sensing Applications. *Adv. Funct. Mater.* **2017**, *27*, 1702695. [CrossRef]
19. Liao, G.; He, F.; Li, Q.; Zhong, L.; Zhao, R.; Che, H.; Gao, H.; Fang, B. Emerging graphitic carbon nitride-based materials for biomedical applications. *Prog. Mater. Sci.* **2020**, *112*, 100666. [CrossRef]
20. Che, S.; Zhang, L.; Wang, T.; Su, D.; Wang, C. Graphitic Carbon Nitride-Based Photocatalysts for Biological Applications. *Adv. Sustain. Syst.* **2022**, *6*, 2100294. [CrossRef]
21. Rono, N.; Kibet, J.K.; Martincigh, B.S.; Nyamori, V.O. A review of the current status of graphitic carbon nitride. *Crit. Rev. Solid State Mater. Sci.* **2021**, *46*, 189–217. [CrossRef]
22. Zheng, Y.; Lin, L.; Wang, B.; Wang, X. Graphitic Carbon Nitride Polymers toward Sustainable Photoredox Catalysis. *Angew. Chem.—Int. Ed.* **2015**, *54*, 12868–12884. [CrossRef] [PubMed]
23. Wang, X.; Blechert, S.; Antonietti, M. Polymeric graphitic carbon nitride for heterogeneous photocatalysis. *ACS Catal.* **2012**, *2*, 1596–1606. [CrossRef]

24. Wang, A.; Wang, C.; Fu, L.; Wong-Ng, W.; Lan, Y. Recent advances of graphitic carbon nitride-based structures and applications in catalyst, sensing, imaging, and leds. *Nano-Micro Lett.* **2017**, *9*, 47. [CrossRef] [PubMed]
25. Gaddam, S.K.; Pothu, R.; Boddula, R. Graphitic carbon nitride (g-C_3N_4) reinforced polymer nanocomposite systems—A review. *Polym. Compos.* **2020**, *41*, 430–442. [CrossRef]
26. Akhundi, A.; Badiei, A.; Ziarani, G.M.; Habibi-Yangjeh, A.; Muñoz-Batista, M.J.; Luque, R. Graphitic carbon nitride-based photocatalysts: Toward efficient organic transformation for value-added chemicals production. *Mol. Catal.* **2020**, *488*, 110902. [CrossRef]
27. Vasiljević, J.; Jerman, I.; Simončič, B. Graphitic carbon nitride as a new sustainable photocatalyst for textile functionalization. *Polymers* **2021**, *13*, 2568. [CrossRef]
28. Jourshabani, M.; Lee, B.K.; Shariatinia, Z. From Traditional Strategies to Z-scheme Configuration in Graphitic Carbon Nitride Photocatalysts: Recent Progress and Future Challenges. *Appl. Catal. B Environ.* **2020**, *276*, 119157. [CrossRef]
29. Wang, F.; Li, W.; Zhang, W.; Ye, R.; Tan, X. Facile fabrication of the Ag nanoparticles decorated graphitic carbon nitride photocatalyst film for indoor air purification under visible light. *Build. Environ.* **2022**, *222*, 109402. [CrossRef]
30. elbakry, S.; Ali, M.E.A.; Abouelfadl, M.; Badway, N.A.; Salam, K.M.M. Effective removal of organic compounds using a novel cellulose acetate coated by PA/g-CN/Ag nanocomposite membranes. *Surf. Interfaces* **2022**, *29*, 101748. [CrossRef]
31. Zedan, M.; Zedan, A.F.; Amin, R.M.; Li, X. Visible-light active metal nanoparticles@carbon nitride for enhanced removal of water organic pollutants. *J. Environ. Chem. Eng.* **2022**, *10*, 107780. [CrossRef]
32. Li, M.; Zhang, J.; He, Y.; Zhang, X.; Cui, Z.; Fu, P.; Liu, M.; Shi, G.; Qiao, X.; Pang, X. Dual enhancement of carrier generation and migration on Au/g-C_3N_4 photocatalysts for highly-efficient broadband PET-RAFT polymerization. *Polym. Chem.* **2022**, *13*, 1022–1030. [CrossRef]
33. Li, H.; Zhang, N.; Zhao, F.; Liu, T.; Wang, Y. Facile fabrication of a novel Au/phosphorus-doped g-C_3N_4 photocatalyst with excellent visible light photocatalytic activity. *Catalysts* **2020**, *10*, 701. [CrossRef]
34. Olatunde, O.C.; Onwudiwe, D.C. A comparative study of the effect of graphene oxide, graphitic carbon nitride, and their composite on the photocatalytic activity of Cu_3SnS_4. *Catalysts* **2022**, *12*, 14. [CrossRef]
35. Ahmad, K.; Kim, H. Design and preparation of g-C_3N_4/rGO modified screen printed electrode for hydrogen peroxide sensing application. *Synth. Met.* **2022**, *286*, 117047. [CrossRef]
36. Li, Y.; Zhang, D.; Chen, Q.; Chao, C.; Sun, J.; Dong, S.; Sun, Y. Synthesis of rGO/g-C_3N_4 for methyl orange degradation in activating peroxydisulfate under simulated solar light irradiation. *J. Alloy. Compd.* **2022**, *907*, 164500. [CrossRef]
37. Hao, D.; Liu, J.; Sun, H.; Fu, B.; Liu, J.; Zhou, J. Integration of g-C_3N_4 into cellulose/graphene oxide foams for efficient photocatalytic Cr(VI) reduction. *J. Phys. Chem. Solids* **2022**, *169*, 110813. [CrossRef]
38. Kobkeatthawin, T.; Chaveanghong, S.; Trakulmututa, J.; Amornsakchai, T.; Kajitvichyanukul, P.; Smith, S.M. Photocatalytic Activity of TiO_2/g-C_3N_4 Nanocomposites for Removal of Monochlorophenols from Water. *Nanomaterials* **2022**, *12*, 2852. [CrossRef]
39. Li, W.; Zhang, H.; Chen, W.; Yang, L.; Wu, H.; Mao, N. The effects of cotton cellulose on both energy band gap of g-C_3N_4–TiO_2 nanoparticles and enhanced photocatalytic properties of cotton-g-C_3N_4–TiO_2 composites. *Cellulose* **2022**, *29*, 193–212. [CrossRef]
40. Girish, Y.R.; Udayabhanu; Alnaggar, G.; Hezam, A.; Nayan, M.B.; Nagaraju, G.; Byrappa, K. Facile and rapid synthesis of solar-driven TiO_2/g-C_3N_4 heterostructure photocatalysts for enhanced photocatalytic activity. *J. Sci. Adv. Mater. Devices* **2022**, *7*, 100419. [CrossRef]
41. Yu, B.; Miao, C.; Wang, D.; Li, H.; Sun, D.; Jiang, W.; Liu, C.; Che, G. Preparation of visible light responsive g-C_3N_4/H-TiO_2 Z-scheme heterojunction with enhanced photocatalytic activity for RhB degradation. *J. Mater. Sci. Mater. Electron.* **2022**, *33*, 17587–17598. [CrossRef]
42. Sundaram, I.M.; Kalimuthu, S.; P, G.P.; Sekar, K.; Rajendran, S. Hierarchical TiO_2 spheroids decorated g-C_3N_4 nanocomposite for solar driven hydrogen production and water depollution. *Int. J. Hydrog. Energy* **2022**, *47*, 3709–3721. [CrossRef]
43. Narkbuakaew, T.; Sattayaporn, S.; Saito, N.; Sujaridworakun, P. Investigation of the Ag species and synergy of Ag-TiO_2 and g-C_3N_4 for the enhancement of photocatalytic activity under UV–Visible light irradiation. *Appl. Surf. Sci.* **2022**, *573*, 151617. [CrossRef]
44. Ibrahim, I.; Belessiotis, G.V.; Antoniadou, M.; Kaltzoglou, A.; Sakellis, E.; Katsaros, F.; Sygellou, L.; Arfanis, M.K.; Salama, T.M.; Falaras, P. Silver decorated TiO_2/g-C_3N_4 bifunctional nanocomposites for photocatalytic elimination of water pollutants under UV and artificial solar light. *Results Eng.* **2022**, *14*, 100470. [CrossRef]
45. Liu, Y.; Yuan, Y.; Ni, S.; Liu, J.; Xie, S.; Liu, Y. Construction of g-C_3N_4/Ag/TiO_2 Z-scheme photocatalyst and Its improved photocatalytic U(VI) reduction application in water. *Water Sci. Technol.* **2022**, *85*, 2639–2651. [CrossRef]
46. Nekooie, R.; Ghasemi, J.B.; Badiei, A.; Shamspur, T.; Mostafavi, A.; Moradian, S. Design and synthesis of g-C_3N_4/(Cu/TiO_2) nanocomposite for the visible light photocatalytic degradation of endosulfan in aqueous solutions. *J. Mol. Struct.* **2022**, *1258*, 132650. [CrossRef]
47. Ding, P.; Ji, H.; Li, P.; Liu, Q.; Wu, Y.; Guo, M.; Zhou, Z.; Gao, S.; Xu, W.; Liu, W.; et al. Visible-light degradation of antibiotics catalyzed by titania/zirconia/graphitic carbon nitride ternary nanocomposites: A combined experimental and theoretical study. *Appl. Catal. B Environ.* **2022**, *300*, 120633. [CrossRef]
48. Sattari, M.; Farhadian, M.; Reza Solaimany Nazar, A.; Moghadam, M. Enhancement of Phenol degradation, using of novel Z-scheme Bi_2WO_6/C_3N_4/TiO_2 composite: Catalyst and operational parameters optimization. *J. Photochem. Photobiol. A Chem.* **2022**, *431*, 114065. [CrossRef]

49. Rashid, M.M.; Simončič, B.; Tomšič, B. Recent advances in TiO_2-functionalized textile surfaces. *Surf. Interfaces* **2021**, *22*, 100890. [CrossRef]
50. Patnaik, S.; Sahoo, D.P.; Parida, K. An overview on Ag modified g-C_3N_4 based nanostructured materials for energy and environmental applications. *Renew. Sustain. Energy Rev.* **2018**, *82*, 1297–1312. [CrossRef]
51. Kavitha, R.; Nithya, P.M.; Girish Kumar, S. Noble metal deposited graphitic carbon nitride based heterojunction photocatalysts. *Appl. Surf. Sci.* **2020**, *508*, 145142. [CrossRef]
52. Simončič, B.; Klemenčič, D. Preparation and performance of silver as an antimicrobial agent for textiles: A review. *Text. Res. J.* **2016**, *86*, 210–223. [CrossRef]
53. Yang, Y.; Guo, Y.; Liu, F.; Yuan, X.; Guo, Y.; Zhang, S.; Guo, W.; Huo, M. Preparation and enhanced visible-light photocatalytic activity of silver deposited graphitic carbon nitride plasmonic photocatalyst. *Appl. Catal. B Environ.* **2013**, *142–143*, 828–837. [CrossRef]
54. Nagajyothi, P.C.; Pandurangan, M.; Vattikuti, S.V.P.; Tettey, C.O.; Sreekanth, T.V.M.; Shim, J. Enhanced photocatalytic activity of Ag/g-C_3N_4 composite. *Sep. Purif. Technol.* **2017**, *188*, 228–237. [CrossRef]
55. Ye, M.; Wang, R.; Shao, Y.; Tian, C.; Zheng, Z.; Gu, X.; Wei, W.; Wei, A. Silver nanoparticles/graphitic carbon nitride nanosheets for improved visible-light-driven photocatalytic performance. *J. Photochem. Photobiol. A Chem.* **2018**, *351*, 145–153. [CrossRef]
56. Paul, D.R.; Sharma, R.; Panchal, P.; Nehra, S.P.; Gupta, A.P.; Sharma, A. Synthesis, characterization and application of silver doped graphitic carbon nitride as photocatalyst towards visible light photocatalytic hydrogen evolution. *Int. J. Hydrog. Energy* **2020**, *45*, 23937–23946. [CrossRef]
57. Luo, T.; Hu, X.; She, Z.; Wei, J.; Feng, X.; Chang, F. Synergistic effects of Ag-doped and morphology regulation of graphitic carbon nitride nanosheets for enhanced photocatalytic performance. *J. Mol. Liq.* **2021**, *324*, 114772. [CrossRef]
58. Wen, K.; Wei, L.; Ren, Z.; Wang, B.; Lu, J. Enhanced photocatalytic degradation of cationic and anionic dyes by Ag-modified g-C_3N_4 composite: Insights on different mechanisms under visible light. *J. Mater. Res.* **2021**, *36*, 1549–1560. [CrossRef]
59. Fontelles-Carceller, O.; Muñoz-Batista, M.J.; Fernández-García, M.; Kubacka, A. Interface Effects in Sunlight-Driven Ag/g-C_3N_4 Composite Catalysts: Study of the Toluene Photodegradation Quantum Efficiency. *ACS Appl. Mater. Interfaces* **2016**, *8*, 2617–2627. [CrossRef]
60. Hak, C.H.; Sim, L.C.; Leong, K.H.; Lim, P.F.; Chin, Y.H.; Saravanan, P. M/g-C_3N_4 (M=Ag, Au, and Pd) composite: Synthesis via sunlight photodeposition and application towards the degradation of bisphenol A. *Environ. Sci. Pollut. Res.* **2018**, *25*, 25401–25412. [CrossRef]
61. Pandiyarajan, C.; Rameshkumar, P.; Murugesan, S.; Selvaraj, M. Silver nanoparticles-supported graphitic-like carbon nitride for the electrochemical sensing of nitrobenzene and its derivatives. *J. Mater. Sci. Mater. Electron.* **2021**, *32*, 19912–19924. [CrossRef]
62. Tian, C.; Tao, X.; Luo, S.; Qing, Y.; Lu, X.; She, J.; Wu, Y. Cellulose nanofibrils anchored Ag on graphitic carbon nitride for efficient photocatalysis under visible light. *Environ. Sci. Nano* **2018**, *5*, 2129–2143. [CrossRef]
63. Song, Y.; Qi, J.; Tian, J.; Gao, S.; Cui, F. Construction of Ag/g-C_3N_4 photocatalysts with visible-light photocatalytic activity for sulfamethoxazole degradation. *Chem. Eng. J.* **2018**, *341*, 547–555. [CrossRef]
64. Minh Tri, N.L.; Kim, J.; Giang, B.L.; Al Tahtamouni, T.M.; Huong, P.T.; Lee, C.; Viet, N.M.; Quang Trung, D. Ag-doped graphitic carbon nitride photocatalyst with remarkably enhanced photocatalytic activity towards antibiotic in hospital wastewater under solar light. *J. Ind. Eng. Chem.* **2019**, *80*, 597–605. [CrossRef]
65. Starukh, H.; Koštejn, M.; Matějka, V.; Praus, P. Graphitic Carbon Nitride as a Platform for the Synthesis of Silver Nanoclusters. *Nanoscale Res. Lett.* **2021**, *16*, 166. [CrossRef]
66. Wang, J.; Cong, J.; Xu, H.; Wang, J.; Liu, H.; Liang, M.; Gao, J.; Ni, Q.; Yao, J. Facile Gel-Based Morphological Control of Ag/g-C_3N_4 Porous Nanofibers for Photocatalytic Hydrogen Generation. *ACS Sustain. Chem. Eng.* **2017**, *5*, 10633–10639. [CrossRef]
67. Muñoz-Batista, M.J.; Fontelles-Carceller, O.; Ferrer, M.; Fernández-García, M.; Kubacka, A. Disinfection capability of Ag/g-C_3N_4 composite photocatalysts under UV and visible light illumination. *Appl. Catal. B Environ.* **2016**, *183*, 86–95. [CrossRef]
68. Khan, M.E.; Han, T.H.; Khan, M.M.; Karim, M.R.; Cho, M.H. Environmentally sustainable fabrication of Ag@g-C_3N_4 nanostructures and their multifunctional efficacy as antibacterial agents and hotocatalysts. *ACS Appl. Nano Mater.* **2018**, *1*, 2912–2922. [CrossRef]
69. Mohanraj, J.; Durgalakshmi, D.; Saravanan, R. Water-soluble graphitic carbon nitride for clean environmental applications. *Environ. Pollut.* **2021**, *269*, 116172. [CrossRef]
70. Cheng, Q.; He, Y.; Ge, Y.; Zhou, J.; Song, G. Ultrasensitive detection of heparin by exploiting the silver nanoparticle-enhanced fluorescence of graphitic carbon nitride (g-C_3N_4) quantum dots. *Microchim. Acta* **2018**, *185*, 332. [CrossRef]
71. Lu, Q.; Wang, H.; Liu, Y.; Hou, Y.; Li, H.; Zhang, Y. Graphitic carbon nitride nanodots: As reductant for the synthesis of silver nanoparticles and its biothiols biosensing application. *Biosens. Bioelectron.* **2017**, *89*, 411–416. [CrossRef]
72. Veerakumar, P.; Rajkumar, C.; Chen, S.M.; Thirumalraj, B.; Lin, K.C. Ultrathin 2D graphitic carbon nitride nanosheets decorated with silver nanoparticles for electrochemical sensing of quercetin. *J. Electroanal. Chem.* **2018**, *826*, 207–216. [CrossRef]
73. Meng, P.; Xu, J. Colorful Silver/Carbon Nitride Composites Obtained by Photoreduction. *Chem. Res. Chin. Univ.* **2020**, *36*, 1136–1140. [CrossRef]
74. Xin, J.; Li, F.; Li, Z.; Zhao, J.; Wang, Y. Controlling the band structure and photocatalytic performance of single atom Ag/C_3N_4 catalysts by variation of silver concentration. *Inorg. Chem. Front.* **2022**, *9*, 302–309. [CrossRef]

75. Fu, Y.; Huang, T.; Zhang, L.; Zhu, J.; Wang, X. Ag/g-C_3N_4 catalyst with superior catalytic performance for the degradation of dyes: A borohydride-generated superoxide radical approach. *Nanoscale* **2015**, *7*, 13723–13733. [CrossRef]
76. Zhao, S.; Wu, J.; Xu, Y.; Wang, Z.; Han, Y.; Zhang, X. Ag_2CO_3-derived Ag/g-C_3N_4 composite with enhanced visible-light photocatalytic activity for hydrogen production from water splitting. *Int. J. Hydrogen Energy* **2020**, *45*, 20851–20858. [CrossRef]
77. Khan, M.R.; Chuan, T.W.; Yousuf, A.; Chowdhury, M.N.K.; Cheng, C.K. Schottky barrier and surface plasmonic resonance phenomena towards the photocatalytic reaction: Study of their mechanisms to enhance photocatalytic activity. *Catal. Sci. Technol.* **2015**, *5*, 2522–2531. [CrossRef]
78. Shah, A.P.; Sharma, A.S.; Sharma, V.S.; Shimpi, N.G. Polyacrylonitrile Nanofibers Incorporating Silver-Decorated Graphitic Carbon Nitride for the Visible-Light-Activated Selective Oxidation of Styrene, Benzylic Methylene Groups, and Benzene. *ACS Appl. Nano Mater.* **2020**, *3*, 1922–1933. [CrossRef]
79. Amedlous, A.; Majdoub, M.; Anfar, Z.; Amaterz, E. Self-supporting g-C_3N_4 nanosheets/Ag nanoparticles embedded onto polyester fabric as "dip-catalyst" for synergic 4-nitrophenol hydrogenation. *Catalysts* **2021**, *11*, 1533. [CrossRef]
80. Bayan, S.; Pal, S.; Ray, S.K. Interface engineered silver nanoparticles decorated g-C_3N_4 nanosheets for textile based triboelectric nanogenerators as wearable power sources. *Nano Energy* **2022**, *94*, 106928. [CrossRef]
81. Yan, H.; Yang, H. TiO_2-g-C_3N_4 composite materials for photocatalytic H_2 evolution under visible light irradiation. *J. Alloy. Compd.* **2011**, *509*, L26–L29. [CrossRef]
82. Zhao, S.; Chen, S.; Yu, H.; Quan, X. g-C_3N_4/TiO_2 hybrid photocatalyst with wide absorption wavelength range and effective photogenerated charge separation. *Sep. Purif. Technol.* **2012**, *99*, 50–54. [CrossRef]
83. Zhang, G.; Zhang, T.; Li, B.; Jiang, S.; Zhang, X.; Hai, L.; Chen, X.; Wu, W. An ingenious strategy of preparing TiO_2/g-C_3N_4 heterojunction photocatalyst: In situ growth of TiO_2 nanocrystals on g-C_3N_4 nanosheets via impregnation-calcination method. *Appl. Surf. Sci.* **2018**, *433*, 963–974. [CrossRef]
84. Jang, E.; Kim, W.J.; Kim, D.W.; Hong, S.H.; Ali, I.; Park, Y.M.; Park, T.J. Atomic layer deposition with rotary reactor for uniform hetero-junction photocatalyst, g-C_3N_4@TiO_2 core-shell structures. *RSC Adv.* **2019**, *9*, 33180–33186. [CrossRef] [PubMed]
85. Mei, P.; Wang, H.; Guo, H.; Zhang, N.; Ji, S.; Ma, Y.; Xu, J.; Li, Y.; Alsulami, H.; Alhodaly, M.S.; et al. The enhanced photodegradation of bisphenol A by TiO_2/C_3N_4 composites. *Environ. Res.* **2020**, *182*, 109090. [CrossRef]
86. Porcu, S.; Castellino, M.; Roppolo, I.; Carbonaro, C.M.; Palmas, S.; Mais, L.; Casula, M.F.; Neretina, S.; Hughes, R.A.; Secci, F.; et al. Highly efficient visible light phenyl modified carbon nitride/TiO_2 photocatalyst for environmental applications. *Appl. Surf. Sci.* **2020**, *531*, 147394. [CrossRef]
87. Ma, J.; Wang, X.; Zong, X.; Li, L.; Sun, H.; He, P.; Yang, Y.; Ding, Y.; Han, Y.; Fan, X. Photoelectrochemical properties of TiO_2/g-C_3N_4 composited electrodes fabricated by a co-electrodeposited method. *J. Phys. D. Appl. Phys.* **2021**, *54*, 145104. [CrossRef]
88. Ranjithkumar, R.; Lakshmanan, P.; Devendran, P.; Nallamuthu, N.; Sudhahar, S.; Kumar, M.K. Investigations on effect of graphitic carbon nitride loading on the properties and electrochemical performance of g-C_3N_4/TiO_2 nanocomposites for energy storage device applications. *Mater. Sci. Semicond. Process.* **2021**, *121*, 105328. [CrossRef]
89. Khan, I.; Khan, S.; Chen, J.; Shah, S.A.; Yuan, A. Biological Inspired Green Synthesis of TiO_2 Coupled g-C_3N_4 Nanocomposites and Its Improved Activities for Sulfadiazine and Bisphenol A Degradation. *J. Clust. Sci.* **2022**. [CrossRef]
90. Liu, Y.; Ren, M.; Zhang, X.; Yang, G.; Qin, L.; Meng, J.; Guo, Y. Supramolecule self-assembly approach to direct Z-scheme TiO_2/g-C_3N_4 heterojunctions for efficient photocatalytic degradation of emerging phenolic pollutants. *Appl. Surf. Sci.* **2022**, *593*, 153401. [CrossRef]
91. Yu, J.; Wang, S.; Low, J.; Xiao, W. Enhanced photocatalytic performance of direct Z-scheme g-C_3N_4-TiO_2 photocatalysts for the decomposition of formaldehyde in air. *Phys. Chem. Chem. Phys.* **2013**, *15*, 16883–16890. [CrossRef]
92. Gu, L.; Wang, J.; Zou, Z.; Han, X. Graphitic-C_3N_4-hybridized TiO_2 nanosheets with reactive {0 0 1} facets to enhance the UV- and visible-light photocatalytic activity. *J. Hazard. Mater.* **2014**, *268*, 216–223. [CrossRef]
93. Li, H.; Zhou, L.; Wang, L.; Liu, Y.; Lei, J.; Zhang, J. In situ growth of TiO_2 nanocrystals on g-C_3N_4 for enhanced photocatalytic performance. *Phys. Chem. Chem. Phys.* **2015**, *17*, 17406–17412. [CrossRef]
94. Tong, Z.; Yang, D.; Xiao, T.; Tian, Y.; Jiang, Z. Biomimetic fabrication of g-C_3N_4/TiO_2 nanosheets with enhanced photocatalytic activity toward organic pollutant degradation. *Chem. Eng. J.* **2015**, *260*, 117–125. [CrossRef]
95. Huang, S.; Zhong, J.; Li, J.; Chen, J.; Xiang, Z.; Hu, W.; Li, M. Z-scheme TiO_2/g-C_3N_4 composites with improved solar-driven photocatalytic performance deriving from remarkably efficient separation of photo-generated charge pairs. *Mater. Res. Bull.* **2016**, *84*, 65–70. [CrossRef]
96. Li, J.; Liu, Y.; Li, H.; Chen, C. Fabrication of g-C_3N_4/TiO_2 composite photocatalyst with extended absorption wavelength range and enhanced photocatalytic performance. *J. Photochem. Photobiol. A Chem.* **2016**, *317*, 151–160. [CrossRef]
97. Kočí, K.; Reli, M.; Troppová, I.; Šihor, M.; Kupkova, J.; Kustrovski, P.; Praus, P. Photocatalytic decomposition of N_2O over TiO_2/g-C_3N_4 photocatalysts heterojunction. *Appl. Surf. Sci.* **2017**, *396*, 1685–1695. [CrossRef]
98. Sun, M.; Shen, S.; Wu, Z.; Tang, Z.; Shen, J.; Yang, J. Rice spike-like g-C_3N_4/TiO_2 heterojunctions with tight-binding interface by using sodium titanate ultralong nanotube as precursor and template. *Ceram. Int.* **2018**, *44*, 8125–8132. [CrossRef]
99. Etacheri, V.; Di Valentin, C.; Schneider, J.; Bahnemann, D.; Pillai, S.C. Visible-light activation of TiO_2 photocatalysts: Advances in theory and experiments. *J. Photochem. Photobiol. C Photochem. Rev.* **2015**, *25*, 1–29. [CrossRef]
100. Nam, Y.; Lim, J.H.; Ko, K.C.; Lee, J.Y. Photocatalytic activity of TiO_2 nanoparticles: A theoretical aspect. *J. Mater. Chem. A* **2019**, *7*, 13833–13859. [CrossRef]

101. Su, F.; Mathew, S.C.; Lipner, G.; Fu, X.; Antonietti, M.; Blechert, S.; Wang, X. mpg-C_3N_4-catalyzed selective oxidation of alcohols using O_2 and visible light. *J. Am. Chem. Soc.* **2010**, *132*, 16299–16301. [CrossRef] [PubMed]
102. Xu, Q.; Zhang, L.; Yu, J.; Wageh, S.; Al-Ghamdi, A.A.; Jaroniec, M. Direct Z-scheme photocatalysts: Principles, synthesis, and applications. *Mater. Today* **2018**, *21*, 1042–1063. [CrossRef]
103. Low, J.; Yu, J.; Jaroniec, M.; Wageh, S.; Al-Ghamdi, A.A. Heterojunction Photocatalysts. *Adv. Mater.* **2017**, *29*, 1601694. [CrossRef] [PubMed]
104. Kumari, P.; Bahadur, N.; Kong, L.; O'Dell, L.A.; Merenda, A.; Dumée, L.F. Engineering Schottky-like and heterojunction materials for enhanced photocatalysis performance—A review. *Mater. Adv.* **2022**, *3*, 2309–2323. [CrossRef]
105. Wang, Y.; Ding, X.; Zhang, P.; Wang, Q.; Zheng, K.; Chen, L.; Ding, J.; Tian, X.; Zhang, X. Convenient and Recyclable TiO_2/g-C_3N_4 Photocatalytic Coating: Layer-by-Layer Self-assembly Construction on Cotton Fabrics Leading to Improved Catalytic Activity under Visible Light. *Ind. Eng. Chem. Res.* **2019**, *58*, 3978–3987. [CrossRef]
106. Chen, Y.; Lu, W.; Shen, H.; Gu, Y.; Xu, T.; Zhu, Z.; Wang, G.; Chen, W. Solar-driven efficient degradation of emerging contaminants by g-C_3N_4-shielding polyester fiber/TiO_2 composites. *Appl. Catal. B Environ.* **2019**, *258*, 117960. [CrossRef]
107. Xiong, Q.; Chen, Y.; Xu, T.; Zhu, Z.; Chen, W.; Lu, W. Highly efficient purification of emerging pollutants and bacteria in natural water by g-C_3N_4-sheltered fibers containing TiO_2. *Appl. Surf. Sci.* **2021**, *559*, 149839. [CrossRef]
108. Ghafoor, S.; Inayat, A.; Aftab, F.; Duran, H.; Kirchhoff, K.; Waseem, S.; Arshad, S.N. TiO_2 nanofibers embedded with g-C_3N_4 nanosheets and decorated with Ag nanoparticles as Z-scheme photocatalysts for environmental remediation. *J. Environ. Chem. Eng.* **2019**, *7*, 103452. [CrossRef]
109. Kuang, J.; Xing, Z.; Yin, J.; Li, Z.; Zhu, Q.; Zhou, W. Surface plasma Ag-decorated single-crystalline TiO_{2-x}(B) nanorod/defect-rich g-C_3N_4 nanosheet ternary superstructure 3D heterojunctions as enhanced visible-light-driven photocatalyst. *J. Colloid Interface Sci.* **2019**, *542*, 63–72. [CrossRef]
110. Sobahi, T.R.; Amin, M.S. Upgrading the photocatalytic achievement of g-C_3N_4 nanosheets along decoration with Ag@TiO_2 nanospheres for the preparation of vitamin B3. *Appl. Nanosci.* **2019**, *9*, 1621–1636. [CrossRef]
111. Ahmed, A.; Niazi, M.B.K.; Jahan, Z.; Ahmad, T.; Hussain, A.; Pervaiz, E.; Janjua, H.A.; Hussain, Z. In-vitro and in-vivo study of superabsorbent PVA/Starch/g-C_3N_4/Ag@TiO_2 NPs hydrogel membranes for wound dressing. *Eur. Polym. J.* **2020**, *130*, 109650. [CrossRef]
112. Mahvelati-Shamsabadi, T.; Lee, B.K. Design of Ag/g-C_3N_4 on TiO_2 nanotree arrays via ultrasonic-assisted spin coating as an efficient photoanode for solar water oxidation: Morphology modification and junction improvement. *Catal. Today* **2020**, *358*, 412–421. [CrossRef]
113. Sui, G.; Li, J.; Du, L.; Zhuang, Y.; Zhang, Y.; Zou, Y.; Li, B. Preparation and characterization of g-C_3N_4/Ag–TiO_2 ternary hollowsphere nanoheterojunction catalyst with high visible light photocatalytic performance. *J. Alloy Compd.* **2020**, *823*, 153851. [CrossRef]
114. Soh, M.F.; Noh, M.F.M.; Mohamed, N.A.; Safaei, J.; Rosli, N.N.; Lim, E.L.; Yap, C.C.; Teridi, M.A.M. Incorporation of g-C_3N_4/Ag dopant in TiO_2 as electron transport layer for organic solar cells. *Mater. Lett.* **2019**, *253*, 117–120. [CrossRef]
115. Yang, Y.; Lu, C.; Ren, J.; Li, X.; Ma, Y.; Huang, W.; Zhao, X. Enhanced photocatalytic hydrogen evolution over TiO_2/g-C_3N_4 2D heterojunction coupled with plasmon Ag nanoparticles. *Ceram. Int.* **2020**, *46*, 5725–5732. [CrossRef]
116. Yu, B.; Meng, F.; Khan, M.W.; Qin, R.; Liu, X. Facile synthesis of AgNPs modified TiO_2@g-C_3N_4 heterojunction composites with enhanced photocatalytic activity under simulated sunlight. *Mater. Res. Bull.* **2020**, *121*, 110641. [CrossRef]
117. Wang, W.; Zhang, D.; Sun, P.; Ji, Z.; Duan, J. High efficiency photocatalytic degradation of indoor formaldehyde by Ag/g-C_3N_4/TiO_2 composite catalyst with ZSM-5 as the carrier. *Microporous Mesoporous Mater.* **2021**, *322*, 111134. [CrossRef]
118. Chen, Y.; Huang, W.; He, D.; Situ, Y.; Huang, H. Construction of heterostructured g-C_3N_4/Ag/TiO_2 microspheres with enhanced photocatalysis performance under visible-light irradiation. *ACS Appl. Mater. Interfaces* **2014**, *6*, 14405–14414. [CrossRef]
119. Wang, C.; Rao, Z.; Mahmood, A.; Wang, X.; Wang, Y.; Xie, X.; Sun, J. Improved photocatalytic oxidation performance of gaseous acetaldehyde by ternary g-C_3N_4/Ag-TiO_2 composites under visible light. *J. Colloid Interface Sci.* **2021**, *602*, 699–711. [CrossRef]
120. Leong, K.H.; Liu, S.L.; Sim, L.C.; Saravanan, P.; Jang, M.; Ibrahim, S. Surface reconstruction of titania with g-C_3N_4 and Ag for promoting efficient electrons migration and enhanced visible light photocatalysis. *Appl. Surf. Sci.* **2015**, *358*, 370–376. [CrossRef]
121. Zang, M.; Shi, L.; Liang, L.; Li, D.; Sun, J. Heterostructured g-C_3N_4/Ag-TiO_2 composites with efficient photocatalytic performance under visible-light irradiation. *RSC Adv.* **2015**, *5*, 56136–56144. [CrossRef]
122. Li, H.; Gao, Y.; Wu, X.; Lee, P.H.; Shih, K. Fabrication of Heterostructured g-C_3N_4/Ag-TiO_2 Hybrid Photocatalyst with Enhanced Performance in Photocatalytic Conversion of CO_2 Under Simulated Sunlight Irradiation. *Appl. Surf. Sci.* **2017**, *402*, 198–207. [CrossRef]
123. Zhou, B.; Hong, H.; Zhang, H.; Yu, S.; Tian, H. Heterostructured Ag/g-C_3N_4/TiO_2 with enhanced visible light photocatalytic performances. *J. Chem. Technol. Biotechnol.* **2019**, *94*, 3806–3814. [CrossRef]
124. Zhou, Y.; Zhao, D.; Cao, F.; Luo, Q.; Xiang, Y.; Deng, Y. Highly photoactive Ag-based urchin-like E-g-C_3N_4 /TiO_2 ternary composite photocatalyst. *Micro Nano Lett.* **2019**, *14*, 154–157. [CrossRef]
125. Jo, W.K.; Yoo, H.J. Combination of ultrasound-treated 2D g-C_3N_4 with Ag/black TiO_2 nanostructure for improved photocatalysis. *Ultrason.—Sonochem.* **2018**, *42*, 517–525. [CrossRef]

126. Geng, R.; Yin, J.; Zhou, J.; Jiao, T.; Feng, Y.; Zhang, L.; Chen, Y.; Bai, Z.; Peng, Q. In Situ Construction of Ag/TiO_2/g-C_3N_4 Heterojunction Nanocomposite Based on Hierarchical Co-Assembly with Sustainable Hydrogen Evolution. *Nanomaterials* **2020**, *10*, 1. [CrossRef]
127. Chai, B.; Peng, T.; Mao, J.; Li, K.; Zan, L. Graphitic carbon nitride (g-C_3N_4)-Pt-TiO_2 nanocomposite as an efficient photocatalyst for hydrogen production under visible light irradiation. *Phys. Chem. Chem. Phys.* **2012**, *14*, 16745–16752. [CrossRef]
128. Tangwongputti, C.; Reubroycharoen, P.; Sujaridworakun, P. Facile synthesis of heterostructured g-C_3N_4/Ag -TiO_2 photocatalysts with enhanced visible-light photocatalytic performance. *J. Met. Mater. Miner.* **2022**, *32*, 48–54. [CrossRef]